UC Berkeley
UC Berkeley Electronic Theses and Dissertations

**Title**
Model-Free Optimal Control of Distributed Energy Resources in Electric Power Distribution Systems

**Permalink**
https://escholarship.org/uc/item/3r30q0tb

**Author**
Arnold, Daniel Brian

**Publication Date**
2015

Peer reviewed|Thesis/dissertation

eScholarship.org Powered by the California Digital Library
University of California

**Model-Free Optimal Control of Distributed Energy Resources in Electric Power Distribution Systems**

by

Daniel B. Arnold

A dissertation submitted in partial satisfaction of the

requirements for the degree of

Doctor of Philosophy

in

Engineering - Mechanical Engineering

in the

Graduate Division

of the

University of California, Berkeley

Committee in charge:

Professor David Auslander, Chair
Assistant Professor Duncan Callaway
Professor Kameshwar Poolla
Associate Professor Alexandra von Meier

Fall 2015

**Model-Free Optimal Control of Distributed Energy Resources in Electric Power Distribution Systems**

Copyright 2015
by
Daniel B. Arnold

## Abstract

Model-Free Optimal Control of Distributed Energy Resources in Electric Power Distribution Systems

by

Daniel B. Arnold

Doctor of Philosophy in Engineering - Mechanical Engineering

University of California, Berkeley

Professor David Auslander, Chair

Distributed Energy Resources (DER) have the potential to both improve the manner in which the electric power distribution system is operated and provide services to the bulk electric grid. A key question that has emerged in academic circles is the manner in which DER is governed to provide such utility. While many of the suggested approaches are mathematically elegant and demonstrate positive performance in simulations, they face enormous barriers to implementation due to their reliance on knowledge of network models and burdensome communications requirements. This dissertation focuses on the application of an Extremum Seeking (ES) control approach to manage individual DER, that does not require utility network models and or communication between agents. Results achieved from the application of this technique are shown to be equivalent to those derived from centrally-based optimization strategies that utilize convex relaxation techniques. Initially, I explore the use of Extremum Seeking to manage reactive power resources to perform voltage constrained optimization in balanced radial distribution systems. Next, also for balanced and radial distribution systems, I extend this work to consider the management of four-quadrant-capable DER to enable voltage-constrained distribution substation real power and voltage reference tracking. My approach essentially allows the distribution feeder to act as a controllable (P,V) bus when viewed from the perspective of the Transmission System Operator. Finally, in an attempt to extend my results to 3-phase distribution systems, I derive a linear approximation to unbalanced power flow and explore a new objective of using reactive power resources to regulate and balance system voltages. While the latter-most piece does not specifically consider ES, it lays the necessary foundation for the application of the approach in unbalanced systems.

For my family

Trying to make this world a better place for you

# Contents

**Contents** **ii**

**List of Figures** **iv**

**List of Tables** **vi**

**1 Introduction** **1**

**2 ES Control of VAR Resources** **5**
2.1 Preface . . . . . 6
2.2 Preliminaries . . . . . 9
2.3 Control Design . . . . . 14
2.4 Simulation Results . . . . . 19
2.5 Concluding Remarks . . . . . 28

**3 ES Control of Four-Quadrant DER** **29**
3.1 Preface . . . . . 30
3.2 Control Design . . . . . 33
3.3 Problem Formulation . . . . . 39
3.4 Simulation Results . . . . . 42
3.5 Concluding Remarks . . . . . 48

**4 Linear OPF Formulation for Unbalanced Systems** **49**
4.1 Preface . . . . . 50
4.2 Preliminaries . . . . . 52
4.3 Derivation of Linearized Model . . . . . 53
4.4 Simulation Results . . . . . 56
4.5 Concluding Remarks . . . . . 62

**5 Conclusions** **63**

**References** **66**

**Bibliography** **69**

**A Appendix** **70**
A.1 Proof of Theorem 1 . . . . . 70
A.2 Discussion of Objective Function for Eq. (3.43) . . . . . 73

# List of Figures

2.1 Block diagram for scalar gradient-based *Extremum Seeking* control algorithm. . 14
2.2 Multiple ES controllers in operating in parallel. . . . . 15
2.3 Feeder model used in simulations [23]. Nodes in red indicate where VAR resources controlled by ES are located. . . . . 19
2.4 Real power demands on the 13 node feeder. . . . . 20
2.5 Reactive power output of controllable VAR resources. The thickness of the line is due to the small perturbation signal of each controller. . . . . 21
2.6 Node 4 voltage profile during the simulation. . . . . 21
2.7 Feeder head reactive power . . . . . 22
2.8 Feeder head real power . . . . . 22
2.9 IEEE 37 node feeder model. . . . . 23
2.10 Feeder head real power . . . . . 25
2.11 Reactive power output of controllable VAR resources. . . . . 26
2.12 Feeder head reactive power. . . . . 26
2.13 Voltage at node 708 profile during the simulation. . . . . 27
2.14 Voltage violations for regulated nodes (711, 708, 744, 718, 742, and 724) during the simulation. . . . . 27

3.1 Block diagram for scalar gradient-based *Extremum Seeking* control algorithm. . 33
3.2 Multiple ES controllers in operating in parallel. . . . . 35
3.3 IEEE 37 node feeder model. . . . . 43
3.4 Feeder head (substation) real power. . . . . 44
3.5 Feeder head (substation) voltage. . . . . 45
3.6 Feeder head (substation) reactive power. . . . . 45
3.7 Reactive power output of controllable DER. . . . . 46
3.8 Real power output of controllable DER. . . . . 46
3.9 Voltage profiles for regulated nodes during the simulation. . . . . 47

4.1 IEEE 13 node feeder model. . . . . 57
4.2 Phase $a$ voltage magnitudes for base and control scenarios plotted individually. Dashed lines represent line segments between nodes. . . . . 59

4.3 Phase $b$ voltage magnitudes for base and control scenarios plotted individually. Dashed lines represent line segments between nodes. . . . . 59
4.4 Phase $c$ voltage magnitudes for base and control scenarios plotted individually. Dashed lines represent line segments between nodes. . . . . 59
4.5 Phase $a$, $b$, and $c$ voltages magnitudes without control. . . . . 60
4.6 Phase $a$, $b$, and $c$ voltages magnitudes with control. . . . . 60
4.7 Phase voltage imbalance for all nodes, defined as the first term in the objective function of (4.23). . . . . 60
4.8 Optimal inverter VAR dispatch according to (4.23). . . . . 61

A.1 Simplified ES block diagram. High pass filter before demodulation and low pass filter after demodulation are neglected. . . . . 74

# List of Tables

2.1 ES simulation parameters for the 13 node feeder experiment. . . . . 20
2.2 37 Node Feeder Line Configurations (see [26] for line segment assignments). Note these values are not p.u.. For this experiment, a base value of $Z_{base} = 9.2\Omega$ was utilized. . . . . 24
2.3 ES simulation parameters for the 37 node feeder experiment. . . . . 25

3.1 37 Node Feeder Line Configurations (see [26] for line segment assignments). Note these values are not p.u.. For this experiment, a base value of $Z_{base} = 9.2\Omega$ was utilized. . . . . 42
3.2 Inverter capacities for controllable DER during the simulation. $S_{cap}$ represents the per unit inverter apparent power capacity. . . . . 43
3.3 ES simulation parameters for the 37 node feeder experiment. . . . . 44

4.1 Spot loads of the 13 node feeder. . . . . 58
4.2 Optimal reactive power output of controllers. . . . . 58

# Acknowledgments

I feel enormously fortunate to have studied controls and power systems at Berkeley over the past 6 years. It has been (and continues to be) an environment that fosters collaboration within and external to the university itself. There are always new approaches and opportunities to be explored given the collection of truly exceptional people gathered here. My only regret is not having more time to chase these ideas.

I cannot possibly hope to sufficiently convey my gratitude to my two main advisers: my dissertaion chair, Dr. David Auslander, and my research adviser, Dr. Duncan Callaway. Thank you both for giving me the freedom to explore new ideas on my own and for being there to listen and guide. You taught me that failures (or what I thought were failures at the time) can be just as important as successes and that both are opportunities that help me to grow as an academic and a professional.

I also am extremely grateful for the mentorship of Prof. Alexandra von Meier, who gave me the opportunity to participate in a groundbreaking research project, and teach power systems. Thank you Sascha for teaching me about leadership and professionalism, and for giving me the opportunity to mentor other students.

I'd also like to acknowledge the contributions of my colleagues and friends, Matias Negrete-Pincetic, Michael Sankur, and Roel Dobbe.. Their insights and feedback have been invaluable to my dissertation research and my growth as an scholar.

Finally, I need to thank Stephanie for her continued encouragement and unwavering support. I couldn't have done this without you.

# Chapter 1

# Introduction

The electric grid is presently undergoing a transformation that has the potential to fundamentally alter the manner in which power is bought and sold and the way that the system is managed from an operational standpoint. The inexorable movement towards the adoption of distributed renewable resources, electric vehicles, battery storage systems, and responsive loads have opened the door to make the very fingertips of the power system act as generators, loads, and miniature grids all rolled into one. From the perspective of a controls engineer, this transition is littered with opportunities to apply our trade and, indeed, academic publications on strategies to manage these newly controllable Distributed Energy Resources (DER) are prolific.

The need for thoughtful approaches to control DER is evident in the problems faced by utilities at the forefront of renewables integration. Challenges primarily lie in managing an aging infrastructure and increasing reliability in the context of variable resources. As more distributed energy resources are incorporated into the system, feeder voltage profiles and power flows must be carefully managed to ensure power of sufficient quality and quantity is available to retail customers at least cost. As has been experienced in Hawaii [1], the negative impact of high levels of distributed PV under current interconnection standards is significant, and has led to financial impacts to both consumers and the utility. DER, under the correct operational control scenarios, can provide numerous benefits to the grid, including voltage support and regulation services. At the moment, the restrictions imposed by IEEE 1547 prevent these resources from broadly providing such utility to the system. However, ongoing efforts to refine this standard, along with California Rule 21, aim to allow more advanced control options for DER.

Many of the strategies propose for managing DER take the form of centrally-based optimization problems (also known as Optimal Power Flow, or OPF, problems). Such approaches are desirable as they can optimize an objective function while ensuring system voltages are maintained within desired tolerances. The work in [2] proposes a combined gradient-based optimization and rule-based search for Volt-Var Optimization in unbalanced distribution systems. The authors of [3] consider voltage regulation and loss minimization in distribution circuits using second order cone relaxations of balanced feeder models. The works of [4] and

[5] consider voltage regulation in distribution networks in the context of power flow through framing the decision process as a semidefinite program. The results of [4] provide conditions under which the semidefinite relaxation of the nonconvex power flow problem is tight in balanced distribution circuits. In [5], semidefinite relaxations are applied to unbalanced distribution systems, but no optimality conditions are provided. For broad utilization, these methods would require coordinating assets of different manufacturers. In addition, many of these strategies require perfect knowledge of feeder characteristics, such as line segment impedance and network configuration. This information may not be readily available to utility operators. Finally, as these frameworks either depend on solving a centralized optimization or rely on information exchange between decision-makers, it would be necessary to develop an infrastructure to collect sensing information (such as real and reactive power demands) and relay data and actuation signals. This would come at a cost and could require the transfer of information across privately owned assets.

In contrast, decentralized strategies generally sacrifice optimality in favor of less reliance on required communications and system models. Turitsyn et al. [6] considered a suite of distributed control strategies for reactive power compensation using four quadrant inverters. The authors concluded that using local information alone is sufficient for voltage regulation, but the incorporating information about real and reactive power flows improves control system performance. The work of [7] studies distributed voltage regulation in the absence of communication, relying on locally obtained information. Their results extend to optimize a cost associated with the use of reactive power. In [8], a two-stage control architecture for voltage regulation is considered where distributed controllers inject power based on local sensitivity measurements, but communicate with neighbors to makeup shortfalls. The authors of [9] study local voltage reference tracking with integral-type controllers, based on local voltage measurements. While their approach is completely decentralized and distributed, reliance on local measurements precludes the controllers from directly addressing problems in other areas of the network. Using a fully decentralized approach, the work of [10] studied the effect of the shape of different inverter volt-var control curves for voltage regulation in high PV penetration scenarios. These works, while relying less on communications and system models than the strategies in the previous paragraph, deal primarily with voltage regulation and not voltage-constrained optimization.

This dissertation studies a method for solving distribution network optimal power flow problems in a manner that admits minimization of objective functions such as those used in central, model-based approaches while maintaining a distributed, model-free control architecture. This approach does not rely on system models, communications between distributed controllers, or large deployments of additional sensors. To achieve this, I utilize a nonlinear control algorithm known as *Extremum Seeking* (ES) [11]. ES has been used in a variety applications including: robotic motion control [12]-[13], photovoltaic MPPT [14], wind energy conversion [15]-[16], and automotive engine control [17]. The algorithm utilizes a periodic probing signal to perform real time optimization by approximating a gradient descent process. The algorithm is shown to converge to a neighborhood around the global optimizer for convex objective functions, the size of which can be adjusted via altering the strength and

speed of the probing signal (though this will affect algorithm performance). Interestingly, ES can also minimize *non-convex* objective functions provided the probing signal is sufficiently large enough to "free" the controller from local minima.

The initial chapters of this dissertation explore the use of ES to control DER in applications of increasing complexity. First, for balanced and radial distribution systems, ES is used to control distributed reactive power resources to regulate system voltages and minimize resistive losses. In this section, I derive sufficient conditions under which the real and reactive powers at every node are convex and *squared* voltage magnitudes are concave, with respect to reactive power injection anywhere on the feeder. These sufficiency conditions can be interpreted as limits on reverse power flow and losses that cannot be exceeded if feeder-head real power is to be minimized using reactive power resources. Typically, these limits are much greater than feasible operating conditions. In simulations, I demonstrate that multiple VAR resources, each controlled by an independent ES algorithm, can supply reactive power to minimize feeder head real power *and* regulate system voltages without any explicit knowledge of the feeder itself. The only sensing information required by the ES controllers are knowledge of feeder head real power, which can be relatively easily broadcast from the substation, and system voltage measurements. With these two contributions together, the method presented is able to identify globally optimal control solutions (as with centralized OPF formulations) while maintaining a decentralized, model-free formulation.

In the second application, again for balanced and radial distribution systems, ES is used to control the dispatch of real and reactive power resources from controllable DER to enable feeder-head real power and voltage target tracking, while simultaneously providing distribution voltage regulation. In effect, this approach makes the distribution feeder act like a controllable (P,V) bus when viewed from the perspective of the transmission system operator. While in the previous situation, the ES algorithm utilized a unique sinusoidal probe to enable reactive power control for individual DER, this application uses this and the orthogonal sinusoid of the same frequency to enable *simultaneous* real and reactive power control. Such controllable DER resources can be physically represented by 4-quadrant power electric inverters associated with PV and battery storage systems. The main property of these devices that is exploited here is their ability to continuously modulate real power and reactive power outputs (as opposed to legacy devices, such as switched capacitor banks) [18]. Obviously, the ability to control the real power output of PV arrays or battery storage systems is dependent on the availability of sufficient solar insolation or battery state of charge. The main contribution of this piece of research is to demonstrate that multiple DER resources, each controlled by an independent ES algorithm, can dispatch real and reactive power to minimize feeder head real power and voltage tracking errors while regulating system voltages, without any explicit knowledge of the feeder itself and without communicating with other ES controllers.

In the last chapter, I lay the groundwork to extend the ES control approach to manage DER in *unbalanced* 3-phase radial distribution systems. A direct application of ES to unbalanced systems is not straightforward due to the absence of suitable linearized 3-phase power flow models. As such, the derivation of a suitable linearization is a necessary first step

before ES, and many other approaches for that matter, can be applied to manage 3-phase systems. This piece of research attempts to fill that void by proposing a novel linearized unbalanced power flow model that can be viewed as an extension of the *LinDistFlow* [19] linear approximation for balanced systems. Using this linear model, I construct an OPF formulation that dispatches reactive power resources from controllable DER to perform voltage balancing and regulation. My results show that the OPF formulation that utilizes the linearized three phase *LinDistFlow* model results in a dispatch of inverter VAR resources that successfully drives system voltages into acceptable regimes and simultaneously balances voltages by reducing magnitude differences between phases. Application of ES to unbalanced distribution systems is not considered in this dissertation, and is left for future work.

This manuscript is organized so that each piece of research that comprises this dissertation is presented as a self-contained element. Individual chapters may be read in any order, though the reader will most likely better understand the increase in problem complexity if these sections are read in order. The rest of the document is organized as follows. Chapter 2 explores the use of ES to control distributed reactive power resources to regulate system voltages and minimize resistive losses. Section 2.2 introduces the power flow model and the objective function for distributed optimization. Additionally, this section provides conditions for the convexity of optimal power flow problems for a generalized balanced radial distribution feeder. Section 2.3 outlines the ES algorithm and provides a convergence analysis for convex objective functions. In Section 2.4, explores the performance of ES-controlled VAR resources in two numerical experiments. The first experiment demonstrates the ability of ES control to perform unconstrained real power minimization for a 13 node distribution system. Results are compared against an existing centralized approach based on a convex relaxation of the problem. The second experiment considers voltage-constrained real power minimization for a larger system with faster demand data and existing legacy voltage control. Chapter 2 concluding remarks are provided in Section 2.5.

Chapter 3 studies the application of ES to manage four-quadrant-capable DER. Section 3.2 introduces the 2-dimensional ES control algorithm used to control DER inverter real and reactive power contributions and provides a convergence analysis for convex objective functions. Section 3.3 discusses the power flow model and the objective function used for distributed optimization target tracking and voltage regulation. Section 3.4 explores the performance of 2D ES-controlled DER resources in numerical simulations. Concluding remarks for this chapter are then provided in Section 3.5.

Chapter 4 explores the development of a novel linearization for unbalanced power flow which, as discussed, lays the foundation for 3-phase ES that will be studied in future work. Section 4.2 introduces a model of nonlinear three phase unbalanced power flow. This model, used in simulations later in the chapter, is also used in the derivation of the linear approximation for three phase power flow in Section 4.3. In Section 4.4, I formulate an OPF to perform voltage regulation and balancing, and discuss results from simulation. Concluding remarks for this chapter are provided in Section 4.5.

Finally, concluding remarks and a discussion of future work is provided in Chapter 5.

# Chapter 2

# ES Control of VAR Resources

Distributed power electronic reactive power sources – such as smart PV inverters – may play an important role in regulating customer voltages and reducing system losses in future distribution systems. Though it is natural to consider model-based optimal control algorithms to coordinate these distributed resources, those strategies typically require relatively large communications capabilities and accurate models. In this chapter I present an alternative way to implement the optimization problem that circumvents these communications and modeling challenges. I utilize an Extremum Seeking (ES) control algorithm to modulate the reactive power output of VAR resources to minimize total real power delivery at the feeder substation subject to voltage magnitude constraints, without an explicit feeder model. To ensure convergence of the ES approach I derive results that guarantee a variety of distribution feeder objective functions are convex over a broad range of power flows. Simulation results demonstrate that the method is equivalent to recently developed convex relaxations used to solve distribution optimal power flow problems.

## 2.1 Preface

Coordination of a diverse set of Distributed Energy Resources (DER) presents many challenges to utility operators, who strive to ensure power of sufficient quality and quantity is available to retail customers at least cost. Such assets can vary in size from residential rooftop PV units to larger PV arrays and, perhaps, battery storage systems located at commercial and industrial sites. As has been experienced in Hawaii [1], the negative impact of high levels of distributed PV under current interconnection standards is significant, and has led to financial impacts to both consumers and the utility. However, distributed generation resources could, under the correct operational control scenarios, provide numerous benefits to the grid, including voltage support and VAR compensation.

Many of the strategies currently under investigation for VAR compensation involve solving centrally-based optimization problems. The work in [2] proposes a combined gradient-based optimization and rule-based search for Volt-Var Optimization in unbalanced distribution systems. The authors of [3] consider voltage regulation and loss minimization in distribution circuits using second order cone relaxations of balanced feeder models. The works of [4] and [5] consider voltage regulation in distribution networks in the context of power flow through framing the decision process as a semidefinite program. The results of [4] provide conditions under which the semidefinite relaxation of the nonconvex power flow problem is tight in balanced distribution circuits. In [5], semidefinite relaxations are applied to unbalanced distribution systems, but no optimality conditions are provided. For broad utilization, these methods would require coordinating assets of different manufacturers. In addition, many of these strategies require perfect knowledge of feeder characteristics, such as line segment impedances and network configuration. This information may not be readily available to utility operators. Finally, as these frameworks either depend on solving a centralized optimization or rely on information exchange between decision-makers, it would be necessary to develop an infrastructure to collect sensing information (such as real and reactive power demands) and relay data and actuation signals. This would come at a cost and could require the transfer of information across privately owned assets.

In contrast, decentralized strategies generally sacrifice optimality in favor of less reliance on required communications and system models. Turitsyn et al. [6] considered a suite of distributed control strategies for reactive power compensation using four quadrant inverters. The authors concluded that using local information alone is sufficient for voltage regulation, but incorporating information about real and reactive power flows improves control system performance. The work of [7] studies distributed voltage regulation in the absence of communication, relying on locally obtained information. Their results extend to optimize the cost of reactive power, but not other objectives. In [8], a two-stage control architecture for voltage regulation is considered where distributed controllers inject power based on local sensitivity measurements, but communicate with neighbors to makeup shortfalls. The authors of [9] study local voltage reference tracking with integral-type controllers, based on local voltage measurements. While their approach is completely decentralized and distributed, reliance on local measurements precludes the controllers from directly addressing problems in other

areas of the network. Using a fully decentralized approach, the work of [10] studied the effect of the shape of different inverter volt-var control curves for voltage regulation in high PV penetration scenarios. These works, while relying less on communications and system models than the strategies in the previous paragraph, deal primarily with voltage regulation and not voltage-constrained optimization.

In this chapter, I propose and evaluate a method for solving distribution network optimal power flow problems in a manner that admits minimization of objective functions such as those used in central, model-based approaches while maintaining a distributed, model-free control architecture. The specific problem addressed is optimal real-time distributed reactive power support and voltage regulation. The proposed approach does not rely on system models, communications between distributed controllers, or large deployments of additional sensors. To achieve this, I utilize a model-free control algorithm known as Extremum Seeking (ES) [11]. ES has been used in a variety applications including: robotic motion control [12]-[13], photovoltaic MPPT [14], wind energy conversion [15]-[16], and automotive engine control [17]. The algorithm utilizes a periodic probing signal to perform real time optimization, and the approach is guaranteed to converge to within a neighborhood around the optimizer. The size of this neighborhood as well as the rate of convergence can be adjusted via altering the strength and speed of the probing signal. Though I am unaware of ES applications in distribution systems, it should be noted that it is common to deliberately inject periodic signals into feeders, for example as in Power Line Carrier (PLC) communications [20], as well as beacon load detection [21].

The following sections address a specific case of ES control applied to VAR compensation. Here, I consider the dispatch of distributed reactive power resources to minimize feeder head real power. Such resources can be physically represented by 4-quadrant power electric inverters associated with PV and battery storage systems. The main property of these devices that is exploited in this work is their ability to continuously modulate reactive power outputs (as opposed to legacy VAR compensation devices, such as switched capacitor banks) [18].

There are several contributions in this work. First, for any balanced radial distribution feeder, I derive sufficient conditions under which the real and reactive powers at every node are convex and *squared* voltage magnitudes are concave, with respect to reactive power injection anywhere on the feeder. These sufficiency conditions can be interpreted as limits on reverse power flow and losses that cannot be exceeded if feeder-head real power is to be minimized using reactive power resources. Typically, these limits are much greater than feasible operating conditions. The second contribution is to demonstrate that multiple VAR resources, each controlled by an independent ES algorithm, can supply reactive power to minimize feeder head real power *and* regulate system voltages without any explicit knowledge of the feeder itself. The only sensing information required by the ES controllers are knowledge of feeder head real power, which can be relatively easily broadcast from the substation, and system voltage measurements. With these two contributions together, the proposed method is able to identify globally optimal control solutions (as with centralized OPF formulations) while maintaining a decentralized, model-free formulation.

This chapter is outlined as follows. Section 2.2 introduces the power flow model and the objective function for distributed optimization. Additionally, this section provides conditions for the convexity of optimal power flow problems for a generalized balanced radial distribution feeder. Section 2.3 outlines the ES algorithm and provides a convergence analysis for convex objective functions. In Section 2.4, I explore the performance of ES-controlled VAR resources in two numerical experiments. The first experiment demonstrates the ability of ES control to perform unconstrained real power minimization for a 13 node distribution system. Results are compared against an existing centralized approach based on a convex relaxation of the problem. The second experiment considers voltage-constrained real power minimization for a larger system with faster demand data and existing legacy voltage control. I then provide concluding remarks for this chapter in Section 2.5.

## 2.2 Preliminaries

### System Model

Let $T = (H, E)$ denote a rooted tree graph representing a balanced radial distribution feeder, where $H$ is the set of nodes of the feeder and $E$ is the set of line segments. Nodes are indexed by $i = 0, 1, \ldots, m$, where $m$ is the order (number of nodes) of the graph $T$. In this formulation, node 0 denotes the feeder head (or substation) and is the root of $T$. The feeder head is treated as an infinite bus, decoupling interactions in the downstream distribution system from the rest of the grid. While the transmission voltage seen at the substation may evolve over time, it is assumed this evolution takes place on a slower timescale than our inverter control action.

For all $i \in H$ let $y_i$ denote the *squared* magnitude of the node voltage. For adjacent nodes $i$ and $j$, the power/voltage relationship is captured by the system:

$$P_i = p_i + \sum_{j:(i,j)\in E} P_j + \frac{r_{ij}}{y_j}\left(P_j^2 + Q_j^2\right) \tag{2.1}$$

$$Q_i = q_i + u_i + \sum_{j:(i,j)\in E} Q_j + \frac{x_{ij}}{y_j}\left(P_j^2 + Q_j^2\right) \tag{2.2}$$

$$y_i = y_j + 2r_{ij}P_j + 2x_{ij}Q_j + \frac{r_{ij}^2 + x_{ij}^2}{y_j}\left(P_j^2 + Q_j^2\right) \quad \forall j : (i,j) \in E. \tag{2.3}$$

Eqs. (2.1)–(2.3) is a reformulation of the *DistFlow* [19] equations. In this system, node $i$ real and reactive power demands are treated as constant power loads and denoted by $p_i$ and $q_i$, respectively. In this convention, positive demand denotes power consumption and negative demand is power injected, or supplied, to the grid. In this formulation, $P_j$ and $Q_j$ represent the real and reactive power that flows into node $j$ from node $i$, over line segment $(i, j)$. The terms $r_{ij}$ and $x_{ij}$ are rectangular components of edge $(i, j)$ electrical impedance and are assumed to be positive. The quantity $u_i$ represents reactive power that can either be sourced or consumed by a VAR resource.

### Problem Formulation

We are interested in solving an optimal reactive power compensation problem, where the objective is to minimize real power supplied by the distribution substation to the rest of the feeder and to regulate system voltages within $\pm 5\%$ of nominal value. Denote the vector of all control inputs as $u$. The problem is defined as:

$$\begin{aligned} \underset{u,y_i,Q_i,P_i}{\text{minimize}} \quad & P_0 \\ \text{subject to} \quad & (2.1)-(2.3), \\ & \underline{y} \leq y_i \leq \overline{y}, \quad i \in H. \end{aligned} \tag{2.4}$$

The equality constraints of problem Eq. (2.4) govern the physics of the real/reactive power and voltage relationship between adjacent buses in the feeder. In general, these are nonlinear and nonconvex. While this program can be relaxed into a convex form (see [3, 5, 4]), such approaches are not well suited to the problem considered here, as the ES control algorithm is feedback-based and does not allow for the relaxation of the physics of the system. An alternative representation of Eq. (2.4) can be obtained through successive substitutions of Eqs. (2.1)–(2.3) into the objective and inequality constraints. This process eliminates all variables $P_i$, $Q_i$, and $y_i$, leaving $u$ as the only decision variable:

$$\begin{aligned} \underset{u}{\text{minimize}} \quad & P_0(u) \\ \text{subject to} \quad & \underline{y} \leq y_i(u) \leq \overline{y}, \quad i \in H. \end{aligned} \tag{2.5}$$

It is now possible to approximate Eq. (2.5) by an unconstrained problem of the form:

$$\underset{u}{\text{minimize}} \quad J(u), \tag{2.6}$$

where

$$J(u) = c_P P_0(u) + c_y g(u), \tag{2.7}$$

where $g(u)$ is the penalty associated with the inequality constraints of Eq. (2.5), with positive constants $c_P$ and $c_y$ that weight the different terms of the objective. As will be show in Section 3.2, ES control can solve Eq. (2.6) if $J(u)$ is convex.

## Convexity

The first major contribution of this chapter is to establish conditions that can be used to guarantee the convexity of $P_0$ for the un-approximated system of (2.1) – (2.3), with respect to $u$. This result is needed to guarantee that ES control algorithms will dispatch reactive power to minimize feeder-head real power. Although this chapter focuses on using reactive power assets to minimize feeder-head real power, the upcoming results generalize to a wide variety of potential objective functions.

It is now shown that all real and reactive powers are convex and all squared voltage magnitudes are concave with respect to injected reactive powers, $u_i$. These results are valid for arbitrary balanced radial distribution networks with heterogeneous impedance ratios (homogeneous impedance ratios greatly simplify the results). These sufficiency conditions hold in the absence of large amounts reverse power flows and line segment losses.

To begin, consider a distribution feeder represented by $T$. Let $m$ represent the order (i.e. number of nodes) of $T$ and let $u$ be the vector of all controllers ($u_i$) at nodes in $H$, where $u = [u_1, \ldots, u_m]^T \in \Re^{m\times 1}$. Without loss of generality, we assume a controller exists at every node in $H$. For a node $i \in H$, denote the Hessians of $P_i$ and $Q_i$ with respect to $u$ as $\nabla_u^2 P_i \in \Re^{m\times m}$, $\nabla_u^2 Q_i \in \Re^{m\times m}$ respectively. In addition, denote the Hessian of $y_i$ with respect to $u$ as $\nabla_u^2 y_i \in \Re^{m\times m}$. Finally, denote the gradients of $P_i, Q_i$, and $y_i$ with respect to $u$ as $\nabla_u P_i \in \Re^{1\times m}$, $\nabla_u Q_i \in \Re^{1\times m}$, and $\nabla_u y_i \in \Re^{1\times m}$ respectively. The following theorem outlines the regions under which the Hessians $\nabla_u^2 P_i$ and $\nabla_u^2 Q_i$ are positive semidefinite and $\nabla_u^2 y_i$ are negative semidefinite.

**Theorem 1.** *Suppose that for all $i, j \in H$, $(i, j) \in E$, where $i$ is electrically upstream (closer to the distribution substation) from $j$, the following assumptions hold: $y_0$ behaves as an infinite bus (i.e., evolves independently of, and on a timescale slower than, $u$), and the variables $P_j$, $Q_j$, and $y_j$ satisfy the following:*

**C1:** $1 + \frac{c_{ij}}{y_j} P_j \geq 0$

**C2:** $1 + \frac{d_{ij}}{y_j} Q_j \geq 0$

**C3:** $1 - \left(\frac{P_j^2+Q_j^2}{y_j^2}\right)\left(r_{ij}^2 + x_{ij}^2\right) \geq 0$

**C4:** $e_{ij} y_j + P_j + \alpha_j Q_j \geq 0$

**C5:** $f_{ij} y_j + \beta_j P_j + Q_j \geq 0$

*where the positive constants $c_{ij}$, $d_{ij}$, $e_{ij}$, $f_{ij}$, $\alpha_i$ and $\beta_i$ are defined according to:*

$$c_{ij} = \max\left[2r_{ij}, \left(\frac{r_{ij}^2 + x_{ij}^2}{r_{ij}}\right)\right] \tag{2.8}$$

$$d_{ij} = \max\left[2x_{ij}, \left(\frac{r_{ij}^2 + x_{ij}^2}{x_{ij}}\right)\right] \tag{2.9}$$

$$e_{ij} = \begin{cases} \frac{1}{2\alpha_j}\frac{1}{r_{ij}} & \text{if} \quad \frac{x_{ij}}{r_{ij}} \geq \alpha_j \\ \frac{1}{2\alpha_j} \cdot \frac{\alpha_i - \alpha_j}{\alpha_i r_{ij} - x_{ij}} & \text{if} \quad \alpha_j > \frac{x_{ij}}{r_{ij}} \end{cases} \tag{2.10}$$

$$f_{ij} = \begin{cases} \frac{1}{2\beta_j}\frac{1}{x_{ij}} & \text{if} \quad \frac{r_{ij}}{x_{ij}} \geq \beta_j \\ \frac{1}{2\beta_j} \cdot \frac{\beta_i - \beta_j}{\beta_i r_{ij} - x_{ij}} & \text{if} \quad \beta_j > \frac{r_{ij}}{x_{ij}} \end{cases} \tag{2.11}$$

*Then the following results hold $\forall i \in H$, where $v$ is any nonzero vector:*

**R1:** $v^T \nabla_u^2 P_i v \geq 0$

**R2:** $v^T \nabla_u^2 Q_i v \geq 0$

**R3:** $v^T \nabla_u^2 y_i v \leq 0$

The proof can be found in the appendix. Constraints **C1**, **C2**, **C4**, and **C5** place bounds on how much reverse power flow (negative $P$ and $Q$) can occur while still guaranteeing the convexity and concavity conditions **R1** - **R3**. Condition **C3** is a bound on the quantity of resistive losses allowable to ensure convexity and concavity conditions. Recall that in the present notation, at any node, $j$ for instance, $P_j$ and $Q_j$ denote the real and reactive power flowing into node $j$. This is also the power flowing in line segment $i, j$ (where $i$ is the parent of $j$) minus losses. It is obvious that the network topology of the system, especially line segment $r/x$ ratios, greatly affects these conditions.

Parameters $c_{ij}$ and $d_{ij}$ are, in the per unit system, typically $\sim 10^{-1}$ (i.e. on the order of 0.1) or less, implying **C1** and **C2** are only exceeded when $P_j$ and $Q_j$ are substantially less than -1 p.u.. A similar conclusion can be drawn from **C3** which, as $r_{ij}^2 + x_{ij}^2$ is typically $\sim 10^{-2}$ or less, is exceeded if $P_j$ and $Q_j$ are substantially greater than or less than 1 and -1 p.u..

The parameters $\alpha_i$ and $\beta_i$ are chosen to account for downstream impedance ratio heterogeneity (i.e. these parameters are determined at the leaves of the feeder first and proceeding up to the feeder head). The choice for these parameters, illustrated in (2.10) - (2.11), reflects a trade-off which must be made between allowable reverse power flowing in a line segment and upstream $\alpha$ and $\beta$. For example, one can choose $\alpha$ and $\beta$ so that the conditions allow more reverse power flow on downstream line segments, but this would require larger values of upstream $\alpha$ and $\beta$.

For a system with *homogeneous* impedance ratios, the most generous choices for $\alpha$ and $\beta$ are: $\alpha = 1/\beta = x/r$, implying $e_{ij} = 1/2x_{ij}$ and $f_{ij} = 1/2r_{ij}$. With this choice **C4** - **C5** become: $y_j + 2r_{ij}P_j + 2x_{ij}Q_j \geq 0$. As, typically, $r_{ij}$ and $x_{ij}$ are $\sim 10^{-1}$ or less in per unit, this constraint, along with **C1** - **C3** allow amounts of reverse power and losses that greatly exceed normal operating conditions.

For systems with *heterogeneous* impedance ratios, it is not always possible to choose $\alpha_i = x_{ij}/r_{ij}$ and $\beta_i = r_{ij}/x_{ij}$. In this situation, effective choices for these parameters are:

$$\alpha_i = \max_{j \in H, (i,j) \in E} \left[ \frac{\alpha_j - 2kr_{ij}}{1 - 2kx_{ij}}, \frac{x_{ij}}{r_{ij}} \right] \tag{2.12}$$

$$\beta_i = \max_{j \in H, (i,j) \in E} \left[ \frac{\beta_j - 2kx_{ij}}{1 - 2kr_{ij}}, \frac{r_{ij}}{x_{ij}} \right], \tag{2.13}$$

with $k > 0$. This simplifies **C4** - **C5**:

$$ky_j + P_j + \alpha_j Q_j \geq 0 \tag{2.14}$$
$$ky_j + \beta_j P_j + Q_j \geq 0, \tag{2.15}$$

via setting $e_{ij} = f_{ij} = k$. In Section IV, using Eqs. (2.12)–(2.13), I will evaluate Eqs. (2.14)–(2.15) with network model parameters to show that the constraints allow for very large amounts of reverse power flow before the sufficiency conditions of the proof are violated.

When the conditions of Theorem 1 hold, one can use **R1** - **R3** to construct the objective functions for ES control. The form we will use in this instance is:

$$J(u) = c_y \sum_{i \in H} \left( \left[ \underline{y} - y_i \right]^+ \right)^2 + c_y \sum_{i \in H} \left( [y_i - \overline{y}]^+ \right)^2 + c_P P_0 \tag{2.16}$$

where the first term keeps voltages above a lower threshold $\underline{y}$, and the second term serves to keep voltages below an upper threshold $\overline{y}$.

## 2.3 Control Design

### Scalar Gradient-Based Extremum Seeking

This section introduces the scalar gradient-based *Extremum Seeking* control algorithm used to control individual VAR resources to solve the problem of Eq. (2.6). A brief overview of the technique is provided for clarity.

The basic scheme for a single gradient-based ES controller is shown in Fig. 2.1. The algorithm injects a sinusoidal perturbation $a\cos\omega t$ into the system, resulting in an objective function $J(u)$ that now consists of two components: DC and oscillatory. The DC component of the objective function output is removed by the washout filter $s/(s+h)$ and the oscillatory part is subsequently multiplied by $\cos\omega t$ and passed through a low-pass filter $l/(s+l)$. The resulting signal, $\hat{\xi}$ is an estimate of the gradient of the objective function with respect to $u$. The gradient estimate is then passed through an integrator $-k/s$ and added to the modulation signal.

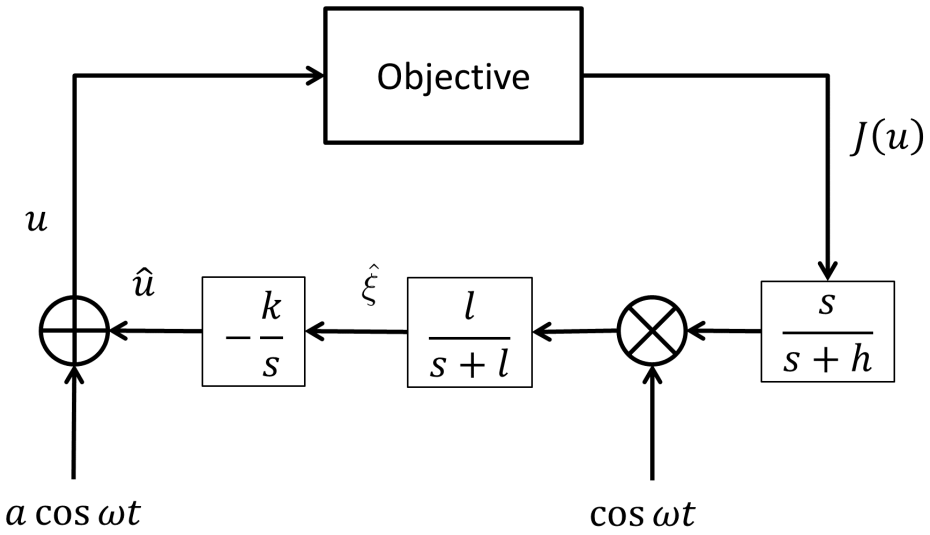



Figure 2.1: Block diagram for scalar gradient-based *Extremum Seeking* control algorithm.

The designer chooses the parameters $\omega$, $l$, and $h$ so that the perturbation is passed by the washout filter, but is removed by the lowpass filter (i.e. $l \ll \omega$ and $h \ll \omega$). [11] shows that if one chooses parameters such that:

$$\omega = \epsilon\omega' \tag{2.17}$$
$$l = \epsilon\delta l' \tag{2.18}$$
$$h = \epsilon\delta h' \tag{2.19}$$
$$k = \epsilon\delta k', \tag{2.20}$$

where $\epsilon$ and $\delta$ are small and positive and $\omega'$, $l'$, $h'$, and $k'$ are $O(1)$ positive real numbers, then for sufficiently small $\epsilon$, $\delta$, and $a$, the output $J(u)$ will converge to an $O(\epsilon + \delta + a)$ neighborhood of $J(u^*)$.

Results of the single controller case of Fig. 2.1 can be extended to allow multiple ES controllers to operate in parallel, as is shown in Fig. 2.2. In the context considered in this chapter, each ES controller (denoted by *ESC* in Fig. 2.2) would represent an individual controllable VAR resource. As outlined in the figure, each controller operates independently of the others, but all utilize the same input signal. To ensure proper convergence of the vector of control inputs $u$ to the optimum $u^*$, it is necessary to choose the perturbation frequencies of the individual controllers such that $\omega_i \neq \omega_j$ and $\omega_i + \omega_j \neq \omega_k$ for distinct $i$, $j$, and $k$. This ensures that the different ES controllers will not "fight" each other during the optimization [11].

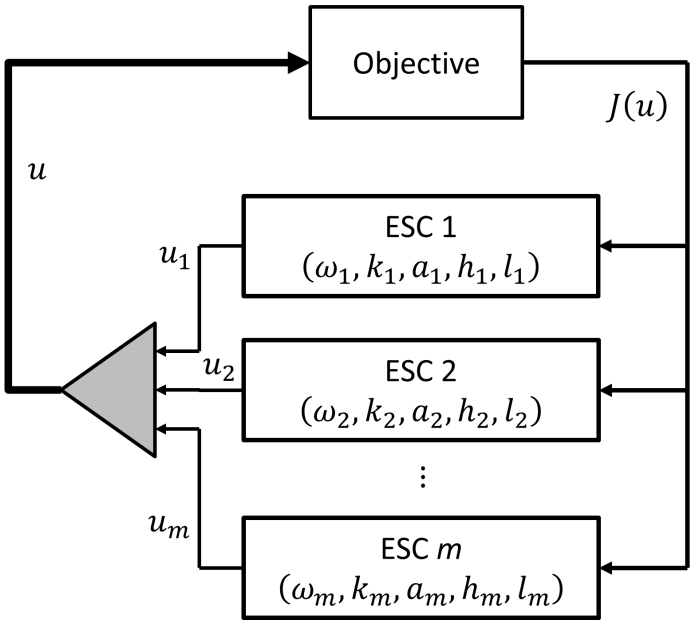



Figure 2.2: Multiple ES controllers in operating in parallel.

## Convergence Analysis

I now provide an analysis showing that the application of ES control to the problem of Eq. (2.6) minimizes the objective Eq. (2.7) to a neighborhood of the optimum.

Consider a convex objective function $J(u)$ with minimizer $u^*$ and define $\phi(u - u^*) = J(u) - J(u^*)$. It is clear that $\phi(u - u^*)$ is convex with minimizer 0 and optimum value 0. Additionally, let $u \in \Re^{m\times 1}$ be the vector of all control inputs, $\hat{u} \in \Re^{m\times 1}$ be the vector consisting of the outputs of the integrator block for each ES controller and $q(t) =$

$[a_1 \cos(\omega_1 t), \ldots, a_m \cos(\omega_m t)]^T$ be the vector containing all perturbation signals. The optimization is performed by placing $m$ ES control loops in parallel as outlined in Figures 2.1 and 2.2. It is assumed that control parameters for each ES loop have been chosen according to Eqs. (2.18)–(2.20) and all probing frequencies have been chosen such that $\omega_i \neq \omega_j$ and $\omega_i + \omega_j \neq \omega_k$ for distinct $i$, $j$, and $k$

In this setting, the vector of control inputs can be expressed as: $u = \hat{u} + q(t)$. For convenience, define the error system $\tilde{u} = \hat{u} - u^*$. Looking now at the $i^{th}$ ES control loop, we have the following nonlinear error dynamics:

$$\dot{e}_i = h_i(\phi(\tilde{u} + q(t)) + J(u^*) - e_i) \tag{2.21}$$
$$\dot{\xi}_i = l_i(-\xi_i + \cos(\omega_i t)(\phi(\tilde{u} + q(t)) + J(u^*) - e_i)) \tag{2.22}$$
$$\dot{\tilde{u}}_i = -k_i \xi_i. \tag{2.23}$$

Let $\tau = \omega_\tau t$ be the lowest common multiple of all time periods in the system such that the entire system is $\tau$-periodic. We may now express the individual probing frequencies as: $\omega_i = \gamma_i \omega_\tau$, where $\gamma_i$ is a positive constant. In the timescale $\tau = \omega_\tau t$, Eqs. (2.21)–(2.23) become:

$$\dot{e}_i = \frac{h_i}{\omega_\tau}(\phi(\tilde{u}) + \nabla_u \phi(\tilde{u}) q(\tau) + J(u^*) - e_i) \tag{2.24}$$
$$\dot{\xi}_i = \frac{l_i}{\omega_\tau}(-\xi_i \cos(\gamma_i \tau)(\phi(\tilde{u}) + \nabla_u \phi(\tilde{u}_i) q(\tau)) \tag{2.25}$$
$$\dot{\tilde{u}}_i = -\frac{k_i}{\omega_\tau}\xi_i, \tag{2.26}$$

where we have approximated $\phi(\tilde{u} + q(t))$ using a Taylor Expansion around $\tilde{u}$. As the system of Eqs. (2.24)–(2.26) is now in the form to which averaging is applicable, we integrate over the period 0 to $\omega_\tau/2\pi$:

$$\dot{e}_{i,av} = \frac{h_i}{2\pi}(\phi_{av}(\tilde{u}_{av}) + J(u^*) - e_{i,av}) \tag{2.27}$$
$$\dot{\xi}_{i,av} = \frac{l_i}{2\pi}\left(-\xi_{i,av} + \frac{a_i}{2\gamma_i}\frac{d\phi_{av}}{du_i}(\tilde{u}_{av})\right) \tag{2.28}$$
$$\dot{\tilde{u}}_{i,av} = -\frac{k_i}{2\pi}\xi_{i,av}, \tag{2.29}$$

where the subscript "av" refers to: $\frac{1}{T}\int_0^T (\cdot) d\tau$ and $T = \frac{\omega_\tau}{2\pi}$. Note the dot notation on the derivative terms refers to $\frac{d}{d\tau}$. The averaging process has removed the sinusoidal term in Eq. (2.27) and extracted the averaged gradient of $\phi$ with respect to $u_i$ (i.e. the input channel to this controller) in Eq. (2.28). The following properties hold for $\phi_{av}(\tilde{u})$ and $\nabla_u \phi_{av}(\tilde{u})$:

$$\phi_{av}(0) = \frac{1}{T}\int_0^T \phi(0)d\tau = 0 \tag{2.30}$$

$$\phi_{av}(u) > 0, \quad \forall u(t) \neq 0 \tag{2.31}$$

$$\phi_{av}(u) \approx \nabla_u \phi_{av}(u)u, \tag{2.32}$$

where Eq. (2.32) results from a Taylor Expansion of $\phi_{av}(0)$. In light of Eqs. (2.30)–(2.32), the system of Eqs. (2.27)–(2.29) has equilibrium at $(e^{eq}_{i,av}, \xi^{eq}_{i,av}, \tilde{u}^{eq}_{i,av}) = (J(u^*), 0, 0)$. At this stage, it is convenient to separate Eqs. (2.27)–(2.29) into two sub-systems: $\dot{e}_{i,av}$ and $(\dot{\xi}_{i,av}, \dot{\tilde{u}}_{i,av})$, as the latter system does not depend on any states of the former. We continue the analysis with the system:

$$\dot{\xi}_{i,av} = \frac{l_i}{2\pi}\left(-\xi_{i,av} + \frac{a_i}{2\gamma_i}\frac{d\phi_{av}}{du_i}(\tilde{u}_{av})\right) \tag{2.33}$$

$$\dot{\tilde{u}}_{i,av} = -\frac{k_i}{2\pi}\xi_{i,av}, \tag{2.34}$$

with equilibrium at the origin. In order to show the averaged dynamics for all ES control loops converge to the origin we seek a Lyapunov function $V(\xi_{av}, \tilde{u}_{av}) = \sum_{i=1}^m V_i(\xi_{i,av}, \tilde{u}_{i,av})$, such that $V > 0$ and $\dot{V} < 0$. It can be verified that choosing $V_i(\xi_{i,av}, \tilde{u}_{i,av})$ such that:

$$V_i(\xi_{i,av}, \tilde{u}_{i,av}) = \frac{1}{2}\begin{bmatrix}\xi_{i,av} & \tilde{u}_{i,av}\end{bmatrix} A_i \begin{bmatrix}\xi_{i,av} \\ \tilde{u}_{i,av}\end{bmatrix} + d\int_0^{\tilde{u}_{i,av}} \frac{d\phi_{av}}{du_i}(\tilde{u}_{av}(y))dy, \tag{2.35}$$

where

$$A_i = \frac{2\gamma_i}{a_i}\begin{bmatrix}\frac{k_i}{l_i}d & -c \\ -c & \frac{l_i}{k_i}c\end{bmatrix}, \tag{2.36}$$

with $d > c > 0$ yields the desired functions:

$$V(\xi_{av}, \tilde{u}_{av}) = \frac{1}{2}\sum_{i=1}^m \begin{bmatrix}\xi_{i,av} & \tilde{u}_{i,av}\end{bmatrix} A_i \begin{bmatrix}\xi_{i,av} \\ \tilde{u}_{i,av}\end{bmatrix} + d\int_0^{\tilde{u}_{av}} \nabla_y \phi_{av}(y)dy \tag{2.37}$$

$$= \frac{1}{2}\sum_{i=1}^m \begin{bmatrix}\xi_{i,av} & \tilde{u}_{i,av}\end{bmatrix} A_i \begin{bmatrix}\xi_{i,av} \\ \tilde{u}_{i,av}\end{bmatrix} + d\phi(\tilde{u}_{av}) \tag{2.38}$$

$$\dot{V}(\xi_{av}, \tilde{u}_{av}) = -\frac{(d-c)}{2\pi}\sum_{i=1}^m \left(\frac{2k_i\gamma_i}{a_i}\right)\xi^2_{i,av} - c\nabla_u \phi_{av}(\tilde{u}_{av})\tilde{u}_{av}, \tag{2.39}$$

where the integral term of Eq. (2.37) is the line integral of a gradient vector (which is equal to $\phi_{av}(\tilde{u}_{av}) - \phi_{av}(0)$), see Eq. (2.38). It is easily verified that Eqs. (2.38) and (2.39) are positive and negative definite respectively, indicating that $V(\xi_{av}, \tilde{u}_{av})$ decreases along the state trajectories of the system (i.e. $\tilde{u}_{av} \to u^*$). Convergence of the vector $u$ to within a neighborhood of $u^*$ is then guaranteed by the proper choice of the ES control parameters and averaging [11], [22].

## 2.4 Simulation Results

### Real Power Minimization

I first illustrate the use of ES control to manage VAR resources to minimize feeder head real power flow. This simulation operates in a range where voltage magnitude constraints are not binding and the objective function *does not* consider voltage constraints. These results will be used to illustrate the ability of the approach to perform model-free decentralized optimization and meaningfully reduce real power supplied by the distribution substation. In the next section I will demonstrate the use of ES control for voltage-constrained distribution system optimization.

Simulations were conducted of ES-managed VAR resources interacting with a 13 node balanced distribution feeder. The feeder model can be found in [23] and is depicted in Fig. 2.3.

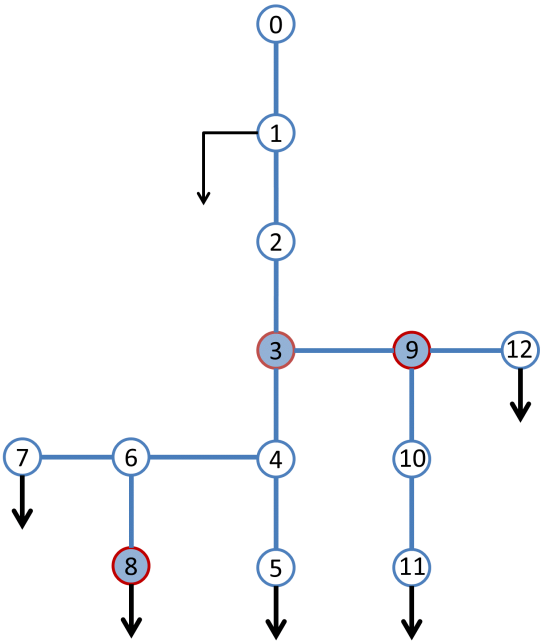



Figure 2.3: Feeder model used in simulations [23]. Nodes in red indicate where VAR resources controlled by ES are located.

This experiment tested the response of multiple ES controllers in the presence of time-varying loads. In this test, VAR resources were located at nodes 3, 8, and 9 and loads were located at nodes 1, 5, 7, 8, 11, and 12. The simulation was driven by publicly available 30 minute demand information (kW) from the Pacific Gas and Electric Company [24] with filtered Gaussian noise added to all real and reactive power demands. This data was interpolated over the duration of a 4 hour experiment with timesteps of 0.1 seconds. A constant power factor of 0.9 was used to create reactive power demand and feeder head voltage was

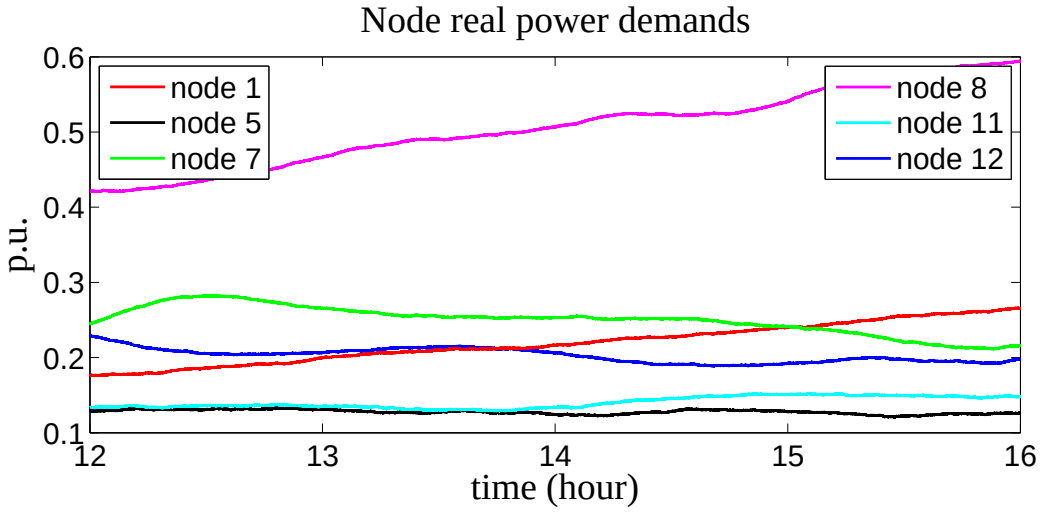



Figure 2.4: Real power demands on the 13 node feeder.

Table 2.1: ES simulation parameters for the 13 node feeder experiment.

| **Node** | **3** | **8** | **9** |
|---|---|---|---|
| $f$ (Hz) | $\frac{\sqrt{2}}{100}$ | $\frac{\sqrt{5}}{100}$ | $\frac{3}{100}$ |
| $h$ ($\frac{rad}{s}$) | $2.5 \times 10^{-3}$ | $2.5 \times 10^{-3}$ | $2.5 \times 10^{-3}$ |
| $l$ ($\frac{rad}{s}$) | $1 \times 10^{-3}$ | $1 \times 10^{-3}$ | $1 \times 10^{-3}$ |
| $k$ | $-7$ | $-7$ | $-7$ |
| $a$ (p.u.) | 0.0075 | 0.0075 | 0.0075 |

fixed to 1 p.u.. The individual real power demand profiles are shown in Fig. 2.4. Feeder base values were 7200 V and 1 MVA, respectively, and all feeder line segments had an impedance of $Z = 0.3 + j0.6\ \Omega$ (or, $0.033 + j0.065\Omega$ p.u.). As this system has homogeneous impedance ratios with impedances that are $\sim 10^{-2}$, one can easily verify that it would require reverse power flows on the order of several times the per unit rating of the feeder to violate conditions **C1** - **C5**. Thus we can conclude that the objective function, $P_0$, is convex. VAR resources were unconstrained by upper and lower limits to demonstrate the ability of the controllers to update in real-time in the presence of time-varying demand. For comparison, the optimal results using the approach of [3] are also plotted. Simulation parameters for the three ES controllers are given in Table 2.1.

Simulation results provided in Figs. 2.5 - 2.8 show the ES controlled VAR resources injecting reactive power into the system and, after an initial settling period, almost perfectly tracking the optimal results. It should be noted that the overshoot and settling time are dependent on the parameter choices for each ES controller and the initial condition. ES

control action results in an improvement in the system voltages (illustrated at node 4, in Fig. 2.6) as well as reductions in reactive and real power supplied to the circuit by the distribution substation (see Figs. 2.7 and 2.8, respectively). Note in Fig. 2.7, the controllers almost completely offset the reactive power supplied to the feeder by the substation.

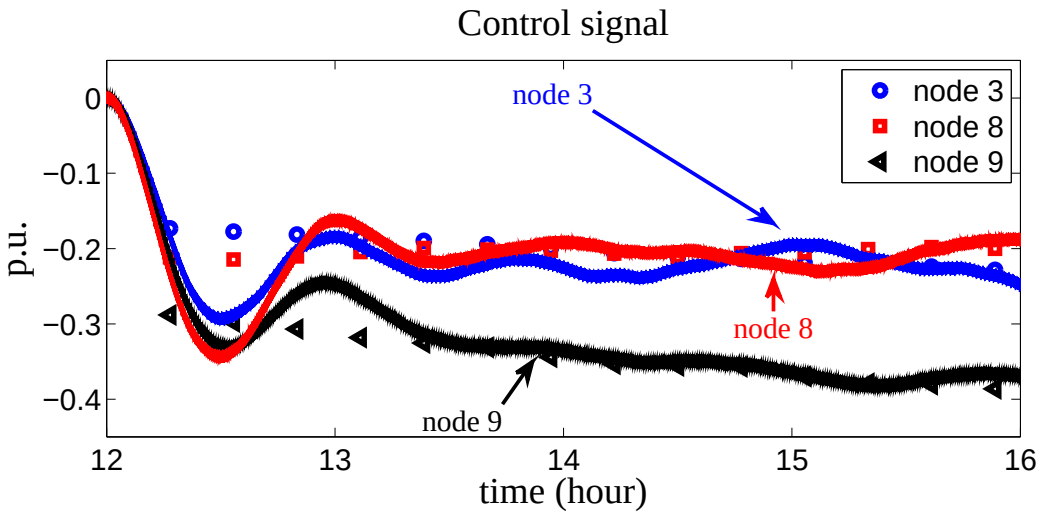



Figure 2.5: Reactive power output of controllable VAR resources. The thickness of the line is due to the small perturbation signal of each controller.

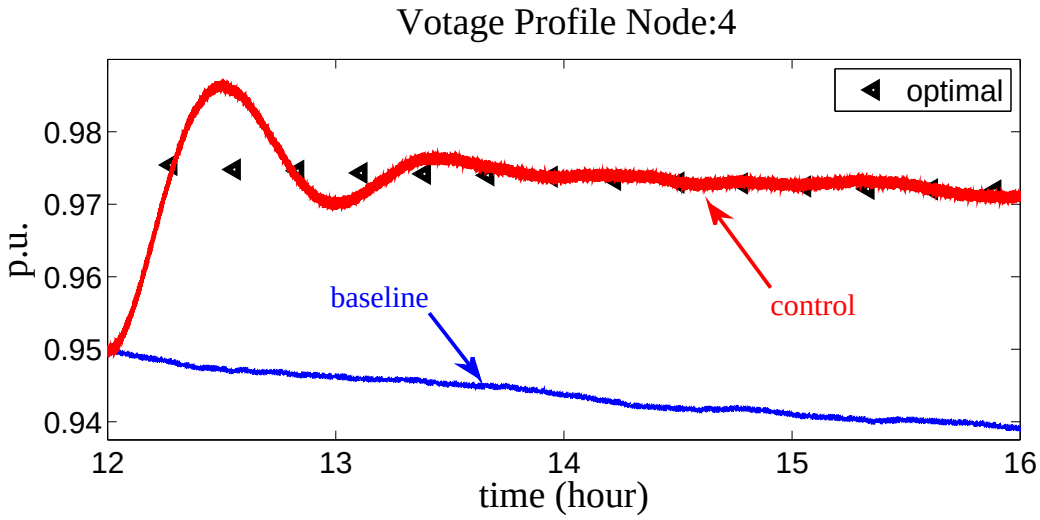



Figure 2.6: Node 4 voltage profile during the simulation.

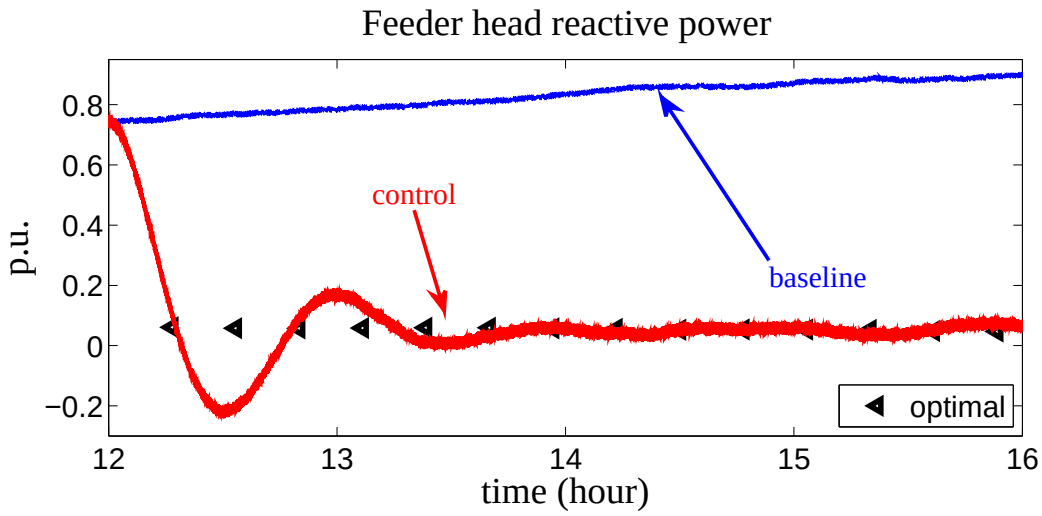



Figure 2.7: Feeder head reactive power

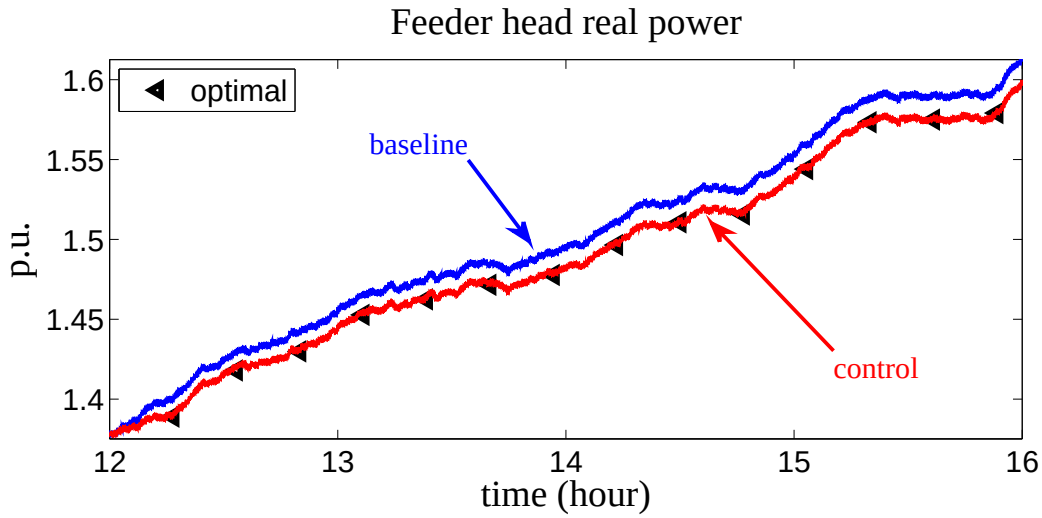



Figure 2.8: Feeder head real power

## Voltage-Constrained Real Power Minimization

In this section I demonstrate the ability of ES control to regulate system voltages during the optimization process. Compared to results presented in the previous section, this experiment utilized much faster (1 minute) demand profiles [25] as well as a larger feeder with capacitor banks that switch independently of ES control actions.

A modified IEEE 37 node distribution feeder model, seen in Fig. 2.9, was utilized in this simulation [26]. The feeder voltage and power ratings were left unchanged (4.8kV and 2.5MVA), as were line segment configuration assignments (see [26]). However, in order to create a balanced network, all line segments were assumed to be three phase with configurations

in Table 2.2.

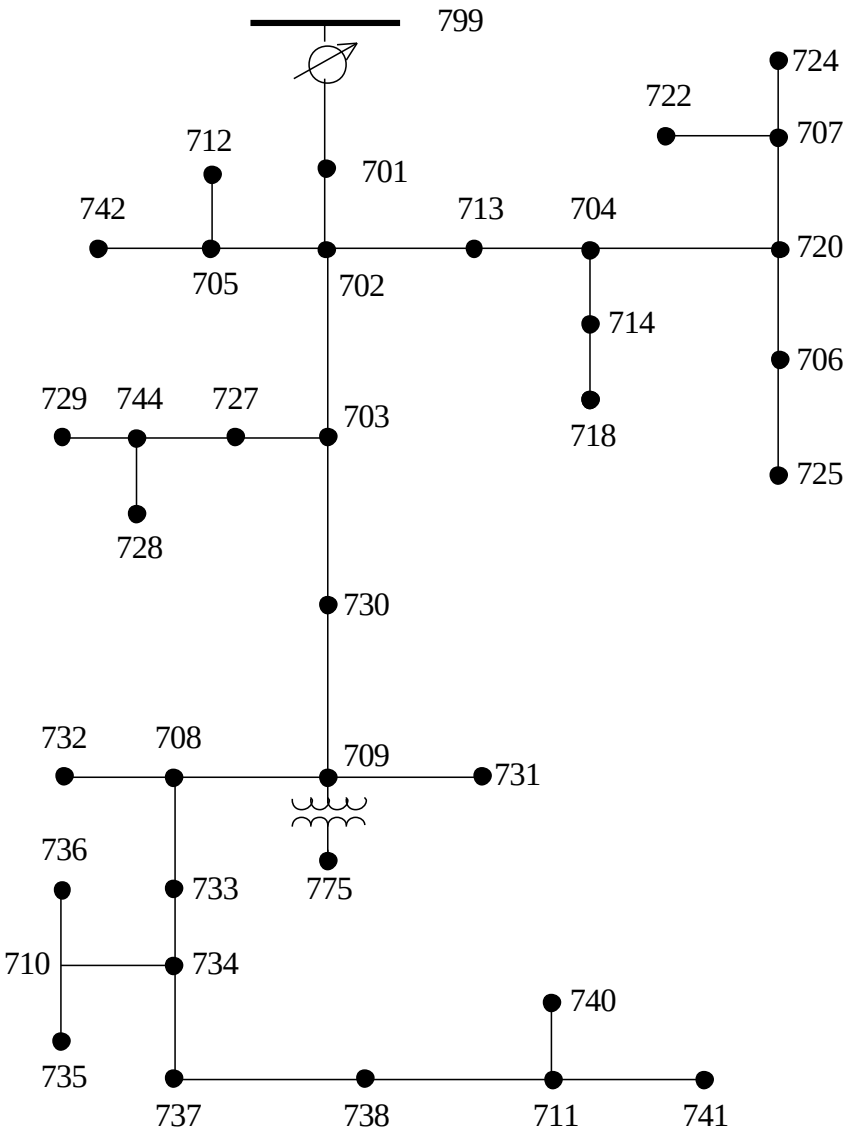



Figure 2.9: IEEE 37 node feeder model.

For this particular feeder configuration per unit impedance values are $\sim 10^{-2}$, thus making **C1** - **C3** unrestrictive. With the given impedance ratios of Table 2.2, one can verify that choosing $k = 4$ and computing the parameters $\alpha$ and $\beta$ according to Eq. (2.12)–(2.13) yields $\alpha_1 = 0.78$ and $\beta_1 = 4.2$. As $\alpha$ and $\beta$ increase moving upstream on the feeder, these values at the first node are always the most restrictive. Considering Eq. (2.14) and Eq. (2.15), Eq. (2.15) is the more restrictive constraint: $4y_1 + 4.2P_1 + Q_1 \geq 0$. Assuming $y_1 \approx 1$, then this constraint is satisfied – and convexity of $P_0$ with respect to $u$ can be guaranteed – even

Table 2.2: 37 Node Feeder Line Configurations (see [26] for line segment assignments). Note these values are not p.u.. For this experiment, a base value of $Z_{base} = 9.2\Omega$ was utilized.

| Configuration | R $\left(\frac{\Omega}{mi}\right)$ | X $\left(\frac{\Omega}{mi}\right)$ | $\frac{x}{r}$ | $\frac{r}{x}$ |
|---|---|---|---|---|
| 721 | 0.592 | 0.394 | 0.66 | 1.50 |
| 722 | 0.95 | 0.891 | 0.94 | 1.07 |
| 723 | 2.588 | 1.342 | 0.52 | 1.93 |
| 724 | 4.19 | 1.55 | 0.37 | 2.70 |

with values of $P_1 = -0.75$ p.u. and $Q_1 = -1$ p.u.. In fact, if $Q_1$ happens to be positive, then even more reverse real power is allowed before losing convexity guarantees.

One minute demand information used in the simulation was obtained from the Pecan St. project [25]. Demand at each node consists of an average of 10 daily load profiles randomly chosen from sites over the period of July 1, 2014 - Aug. 1, 2014. In order to test the performance of the ES approach in scenarios of high renewables penetration, 40% (4 out of 10) of the load profiles at each node came from sites with PV generation. A constant power factor of 0.9 was used to create reactive power demands.

In this simulation, ES controllers were placed at nodes: 711, 708, 744, 718, 742, and 724. In addition, these nodes were also monitored for voltage regulation within ± 5% of feeder head voltage. Parameters of individual ES controllers can be found in Table 2.3, and parameters of the objective function were: $c_P = 10$, $c_y = 500$, $\underline{y} = 0.955^2$, and $\bar{y} = 1.045^2$. Note that the voltage threshold values are tighter than ± 5% to prevent voltages from crossing the 5% limit (had these values been set at ± 5%, the ES controllers would only take action when the voltage was exceeded.). In addition, the transformer at node 775 was replaced by a capacitor bank with a 0.1 p.u. rating, which was activated halfway through the simulation.

Figures 2.10 – 2.14 depict results from a two hour simulation from 14:00 to 16:00 with timesteps of 0.1 seconds with a fixed feeder head voltage of 1 p.u. For comparison, optimal results using a second order cone relaxation technique [3] are also shown (with voltage constraints set at ± 5%). As the results show voltage-constrained ES control is able to substantially offset the amount of reactive power supplied to the feeder by the substation and drive system voltages to within acceptable ranges (see Figs. 2.13 and 2.14). In addition, note substantial reduction in variability of the voltage profile in Fig. 2.13. Figure 2.14 depicts the number of voltage violations (for the set of regulated voltages only) of the ± 5% threshold throughout the experiment. It should also be noted that the step change in reactive power due to capacitor action at 15:00 had no destabilizing effects on ES control.

Table 2.3: ES simulation parameters for the 37 node feeder experiment.

| **Node** | **711** | **708** | **744** | **718** | **742** | **724** |
|---|---|---|---|---|---|---|
| $f$ (Hz) | 1.9 | $\sqrt{3}$ | 1.8 | $\frac{\sqrt{11}}{2}$ | 2.1 | 2.5 |
| $h$ ($\frac{rad}{s}$) | 0.0001 | 0.0001 | 0.0001 | 0.0001 | 0.0001 | 0.0001 |
| $l$ ($\frac{rad}{s}$) | 0.025 | 0.025 | 0.025 | 0.025 | 0.025 | 0.025 |
| $k$ | -10 | -10 | -10 | -10 | -10 | -10 |
| $a$ (p.u.) | 0.0005 | 0.0005 | 0.0005 | 0.0005 | 0.0005 | 0.0005 |

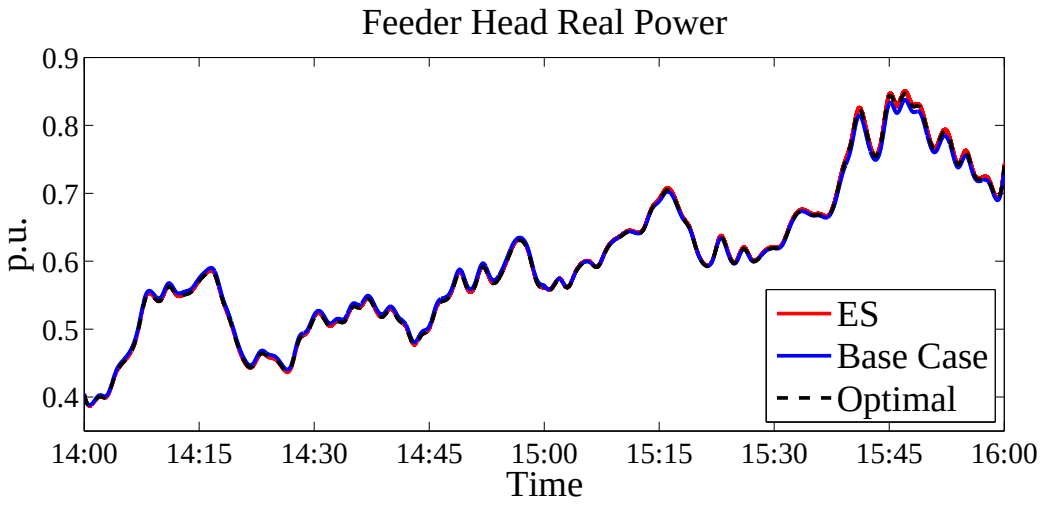



Figure 2.10: Feeder head real power

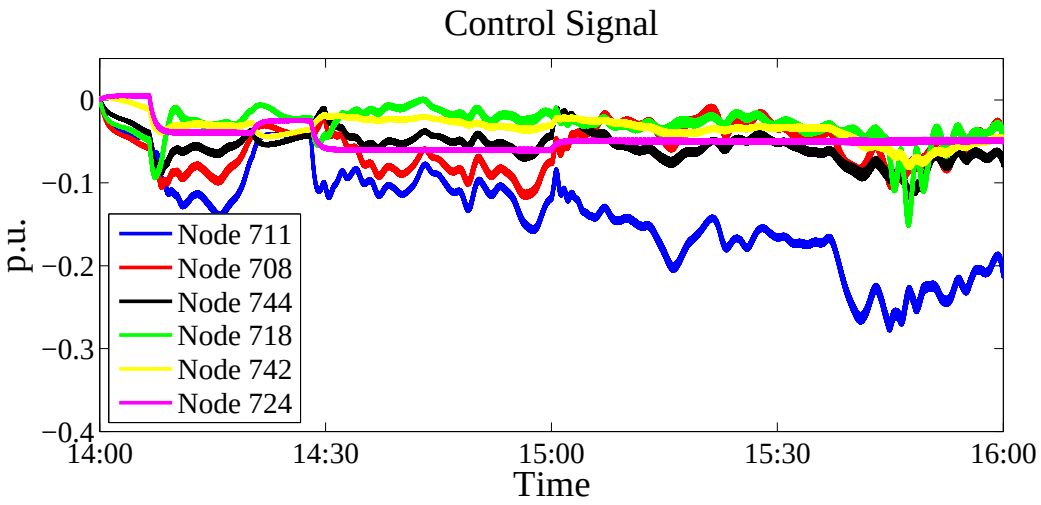



Figure 2.11: Reactive power output of controllable VAR resources.

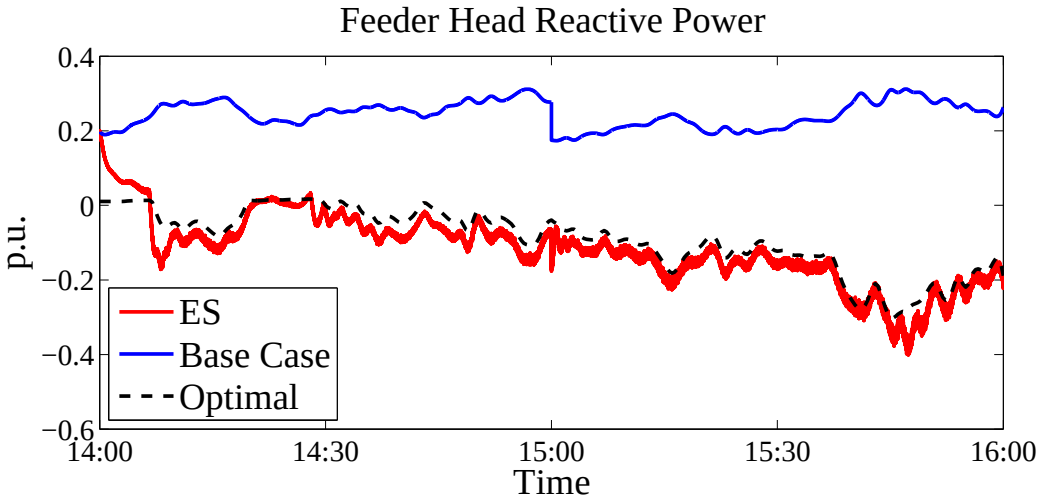



Figure 2.12: Feeder head reactive power.

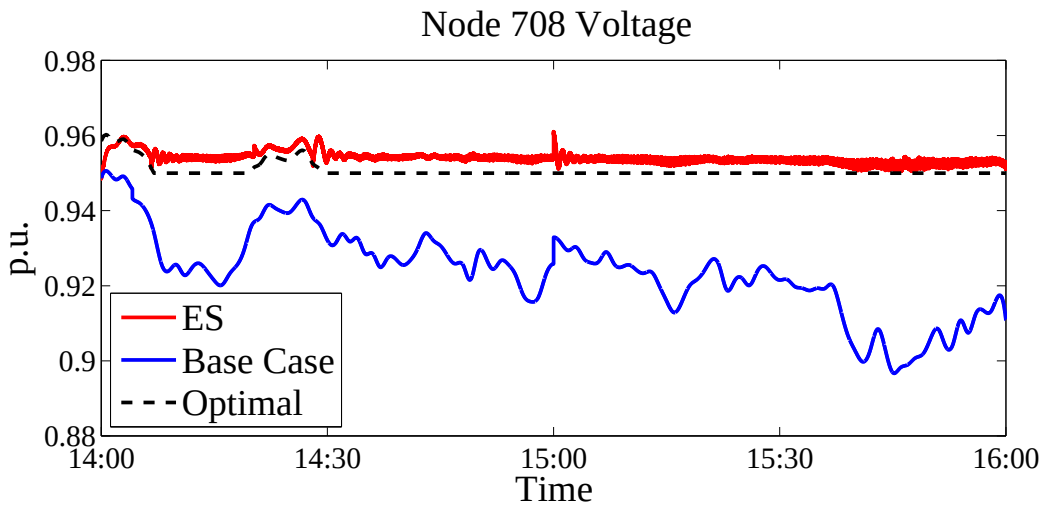



Figure 2.13: Voltage at node 708 profile during the simulation.

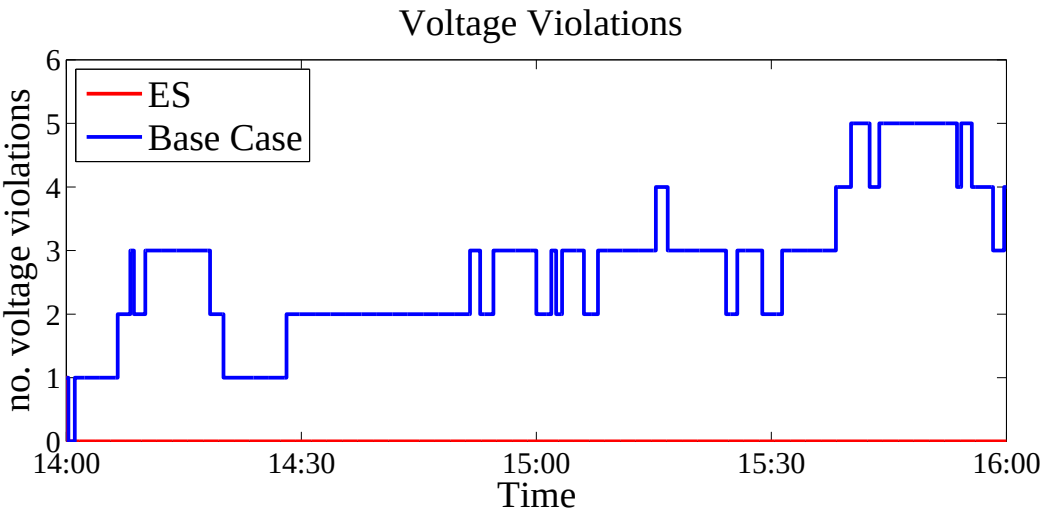



Figure 2.14: Voltage violations for regulated nodes (711, 708, 744, 718, 742, and 724) during the simulation.

## 2.5 Concluding Remarks

This work explored distributed model-free optimization of distribution systems using reactive power assets. There are two main contributions of this research. First, for balanced radial distribution systems, I derived conditions that guarantee feeder real and reactive power flows are convex and *squared* voltage magnitudes are concave with respect to injected reactive powers anywhere on a feeder. These conditions require that *reverse* real and reactive power flows and apparent power magnitudes remain below values that are extremely unlikely to occur on appropriately sized infrastructure. These results are based on the exact balanced distribution power flow equations (i.e. no approximations are required). The second major result is to demonstrate that ES control can manage distributed reactive power resources to perform optimal voltage-constrained real power minimization. This optimization operates in real time, without knowledge of any system models and with purely local decision-making.

In this work, I focused on applications with independent controllers that require relatively little communication. However, centralized multivariable ES may have better performance [14]. The convergence results still hold for this application, and in situations where high amounts of communication and a centralized architecture are acceptable, a multivariable approach may be preferable.

Although the specifics of the hardware providing optimal VAR support were not considered in the analysis and simulation sections, the ES control approach could be utilized by advanced power inverters associated with PV, electric vehicle, and battery storage systems. Such devices have the potential to modulate their power outputs on timescales suitable for ES control and can either provide their own independent probes and/or share probing responsibilities with neighbors. However, it is also possible to extend the approach to control legacy VAR support equipment incapable of actuating on timescales required for ES probing. To do so, it would be necessary to utilize the probing signal from another piece of hardware such as nearby inverters or a dedicated probing resource.

This work constitutes an important step towards practical implementation of distribution optimal power flow. While several existing studies already consider distributed and model-free voltage regulation, this contribution allows for a variety of objectives to be optimized, while ensuring voltages remain acceptable. Moving forward, there are several areas in need of further study. First, it is naturally desirable to extend the results in this work to loads other than constant power. In preliminary analytical and simulation work I have seen that convexity results are lost if a high fraction of loads are voltage dependent; I intend to exactly quantify this fraction in future work. Secondly, an extension of the current approach to unbalanced distribution systems is worth investigating. As the unbalanced power flow equations are considerably more complex than the balanced case, it is not expected to be able to derive sufficient conditions similar to Theorem 1. However, one may study approximate system behavior using suitable linearized power flow models. Though not considered explicitly in this dissertation, Chapter 4 lays the groundwork for 3-phase ES through deriving such a linearization.

# Chapter 3

# ES Control of Four-Quadrant DER

Collective control of Distributed Energy Resources (DER) – such as smart PV inverters – may play an important role in providing regulation services to the bulk electric grid. Though it is natural to consider model-based optimal control algorithms to coordinate these distributed resources for this purpose, those strategies typically require relatively large communications capabilities and accurate network models. In this chapter, I present an alternative way to implement the optimization problem that circumvents these communications and modeling challenges. I present a 2-dimensional Extremum Seeking (ES) control algorithm to modulate the real and reactive power output of DER to enable feeder substation real power and voltage reference tracking subject to voltage magnitude constraints, without an explicit feeder model. From the perspective of the transmission grid, this approach essentially transforms the distribution feeder into a controllable (P,V) bus. Simulation results confirm the ability of the approach to track substation real power and voltage reference signals while maintaining distribution system voltages within acceptable tolerances.

## 3.1 Preface

Coordination of a diverse set of Distributed Energy Resources (DER) presents many challenges to system operators, who strive to ensure power of sufficient quality and quantity is available to retail customers at least cost. Such assets can vary in size from residential rooftop PV units to larger PV arrays and, perhaps, battery storage systems located at commercial and industrial sites. As has been experienced in Hawaii [1], the negative impact of high levels of distributed PV under current interconnection standards is significant, and has led to financial impacts to both consumers and the utility. However, distributed generation resources could, under the correct operational control scenarios, provide numerous benefits to the grid, including voltage support and VAR compensation at the distribution level, and regulation services at the transmission level.

Many of the strategies currently under investigation for coordinating DER involve solving centrally-based optimization problems. The work in [2] proposes a combined gradient-based optimization and rule-based search for Volt-Var Optimization in unbalanced distribution systems. The authors of [3] consider voltage regulation and loss minimization in distribution circuits using second order cone relaxations of balanced feeder models. The works of [4] and [5] consider voltage regulation in distribution networks in the context of power flow through framing the decision process as a semidefinite program. The results of [4] provide conditions under which the semidefinite relaxation of the nonconvex power flow problem is tight in balanced distribution circuits. In [5], semidefinite relaxations are applied to unbalanced distribution systems, but no optimality conditions are provided. For broad utilization, these methods would require coordinating assets of different manufacturers. In addition, many of these strategies require perfect knowledge of feeder characteristics, such as line segment impedances and network configuration. This information may not be readily available to utility operators. Finally, as these frameworks either depend on solving a centralized optimization or rely on information exchange between decision-makers, it would be necessary to develop an infrastructure to collect sensing information (such as real and reactive power demands) and relay data and actuation signals. This would come at a cost and could require the transfer of information across privately owned assets.

In contrast, decentralized strategies generally sacrifice optimality in favor of less reliance on required communications and system models. Turitsyn et al. [6] considered a suite of distributed control strategies for reactive power compensation using four quadrant inverters. The authors concluded that using local information alone is sufficient for voltage regulation, but the incorporating information about real and reactive power flows improves control system performance. The work of [7] studies distributed voltage regulation in the absence of communication, relying on locally obtained information. Their results extend to optimize the cost of reactive power, but the proposed framework does not consider providing feeder-level regulation services. In [8], a two-stage control architecture for voltage regulation is considered where distributed controllers inject power based on local sensitivity measurements, but communicate with neighbors to makeup shortfalls. The authors of [9] study local voltage reference tracking with integral-type controllers, based on local voltage measurements. While

their approach is completely decentralized and distributed, reliance on local measurements precludes the controllers from directly addressing problems in other areas of the network. Using a fully decentralized approach, the work of [10] studied the effect of the shape of different inverter volt-var control curves for voltage regulation in high PV penetration scenarios. These works, while relying less on communications and system models than the strategies in the previous paragraph, deal primarily with voltage regulation and not voltage-constrained optimization.

In this chapter, I propose and evaluate a method for solving distribution network optimal power flow problems in a manner that admits minimization of objective functions such as those used in central, model-based approaches while maintaining a distributed, model-free control architecture. The specific problem addressed is optimal feeder-head real power and voltage reference tracking subject to distribution system voltage constraints. This approach does not rely on system models, communications between distributed controllers, or large deployments of additional sensors. To achieve this, I utilize a model-free control algorithm known as Extremum Seeking (ES) [11]. While Chapter 2 explored the use of ES to conduct model-free optimal VAR compensation and voltage regulation, ES has been used in a variety of other applications including: robotic motion control [12]-[13], photovoltaic MPPT [14], wind energy conversion [15]-[16], and automotive engine control [17]. The algorithm utilizes a periodic probing signal to perform real time optimization, and the approach is guaranteed to converge to within a neighborhood around the optimizer. The size of this neighborhood as well as the rate of convergence can be adjusted via altering the strength and speed of the probing signal. Though I am unaware of ES applications in distribution systems, it should b noted that it is common to deliberately inject periodic signals into distribution systems, for example as in Power Line Carrier (PLC) communications [20], as well as beacon load detection [21].

This chapter considers the dispatch of real and reactive power resources from controllable DER to enable feeder-head real power and voltage target tracking, while simultaneously providing distribution voltage regulation. In effect, this approach makes the distribution feeder act like a controllable (P,V) bus when viewed from the perspective of the transmission system operator. While previously, ES was used to manage power electronic inverter *reactive* power output, this work considers control both the real and reactive power output of an inverter *simultaneously*. Such controllable DER resources can be physically represented by 4-quadrant-capable Distributed Energy Resources such as PV and battery storage systems. The main property of these devices that is exploited in this work is their ability to continuously modulate real power and reactive power outputs (as opposed to legacy devices, such as switched capacitor banks) [18]. Obviously, the ability to control the real power output of PV arrays or battery storage systems is dependent on the availability of sufficient solar insolation or battery state of charge.

The main contribution of this work is to demonstrate that multiple DER resources, each controlled by an independent ES algorithm, can smartly supply real and reactive power to minimize feeder head real power and voltage tracking errors and regulate system voltages, without any explicit knowledge of the feeder itself and without communicating with other

ES controllers. The only sensing information required by the ES controllers are knowledge of substation voltage and real power consumption, which can be relatively easily broadcast from the substation, and system voltage measurements. While in Chapter 2, the ES algorithm utilized a unique sinusoidal probe to enable reactive power control for an individual inverter, this work uses this and the orthogonal sinusoid of the same frequency to enable simultaneous real and reactive power control. The method presented is able to make the distribution feeder act as a controllable (P,V) bus while maintaining a decentralized, model-free formulation.

This chapter is outlined as follows. Section 3.2 introduces the 2-dimensional ES control algorithm used to control DER inverter real and reactive power contributions and provides a convergence analysis for convex objective functions. Section 3.3 discusses the power flow model and the objective function used for distributed optimization target tracking and voltage regulation. Section 3.4 explores the performance of 2D ES-controlled DER resources in numerical simulations. I then provide concluding remarks for this chapter in Section 3.5.

## 3.2 Control Design

This section discusses the two-dimensional scalar gradient-based *Extremum Seeking* algorithm used to control individual DER resources. I now provide an overview of the technique for clarity, followed by a convergence analysis for a convex objective function.

### 2-D Scalar Gradient-Based Extremum Seeking

The scheme for a single 2-D gradient-based ES controller is shown in Fig. 3.1. In this situation, we seek to minimize an objective that is a function of two variables: $u$ and $v$. In the context of this work, $u$ represents controllable real power of a DER and $v$ represents controllable reactive power. The algorithm injects orthogonal sinusoidal perturbations of $a\cos\omega t$ into channel $u$ and $a\sin\omega t$ into channel $v$. This results in an objective function $J(u,v)$ that now consists of two components: DC and oscillatory. The DC component of the objective function output is removed by the washout filter $s/(s+h)$ and the oscillatory part is split into two channels and subsequently multiplied by $\cos\omega t$ (in channel $u$) and by $\sin\omega t$ (in channel $v$). Post-modulation, each signal is passed through a low-pass filter $l/(s+l)$. We note that it is not necessary that the lowpass filter in each channel have the same critical frequency. The resulting signals, $\hat{\xi}_u$ and $\hat{\xi}_v$, are estimates of the gradient of the objective function with respect to $u$ and $v$, respectively. The gradient estimate in each channel is then passed through integrators $-k_u/s$ and $-k_v/s$ and added to its respective modulation signal.

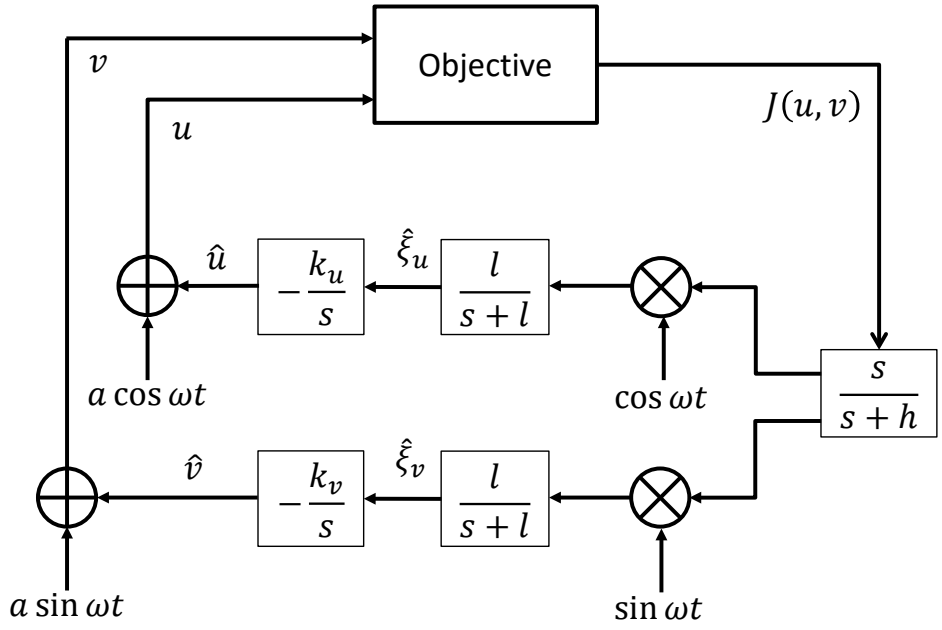



Figure 3.1: Block diagram for scalar gradient-based *Extremum Seeking* control algorithm.

The designer chooses the parameters $\omega$, $l$, and $h$ so that the perturbation is passed by the washout filter, but is removed by the lowpass filter (i.e. $l \ll \omega$ and $h \ll \omega$). It is straightforward to extend the analysis of [11] to show that if one chooses parameters such that:

$$\omega = \epsilon\omega' \tag{3.1}$$
$$l = \epsilon\delta l'$$
$$h = \epsilon\delta h'$$
$$k_u = \epsilon\delta k'_u$$
$$k_v = \epsilon\delta k'_v, \tag{3.2}$$

where $\epsilon$ and $\delta$ are small and positive and $\omega'$, $l'$, $h'$, $k'_u$, and $k'_v$ are $O(1)$ positive real numbers, then for sufficiently small $\epsilon$, $\delta$, and $a$, the output $J(u, v)$ will converge to an $O(\epsilon + \delta + a)$ neighborhood of $J(u^*, v^*)$.

Results of the single controller case of Fig. 3.1 can be extended to allow multiple 2-D ES controllers to operate in parallel, as is shown in Fig. 3.2. In the context considered in this research, each ES controller (denoted by *ESC* in Fig. 3.2) would represent an individual controllable DER resource capable of simultaneously modulating its real and reactive power output. As outlined in the figure, each controller operates independently of the others, but all utilize the same input signal. To ensure proper convergence of the vector of control inputs $[u, v]$ to a neighborhood of the optimum $(u^*, v^*)$, it is necessary to choose the perturbation frequencies of the individual controllers such that $\omega_i \neq \omega_j$ and $\omega_i + \omega_j \neq \omega_k$ for distinct $i$, $j$, and $k$. This ensures that the different ES controllers will not "fight" each other during the optimization [11].

## Convergence Analysis

I now provide an analysis showing that 2D ES control will minimize a convex objective function of two variables. The optimization is performed by placing $m$ ES control loops in parallel as outlined in Figures 3.1 and 3.2. It is assumed that control parameters for each ES loop have been chosen according to Eqs. (3.1)–(3.2) and all probing frequencies have been chosen such that $\omega_i \neq \omega_j$ and $\omega_i + \omega_j \neq \omega_k$ for distinct $i$, $j$, and $k$. To begin, consider a convex objective function of two variables $J(u, v)$ with minimizer $[u^*, v^*]$ and define $\phi(u - u^*, v - v^*) = J(u, v) - J(u^*, v^*)$. It is clear that $\phi$ is convex with minimizer $(0, 0)$ and optimum value 0. Additionally, let $u \in \Re^{m\times 1}$ and $v \in \Re^{m\times 1}$ be the vectors of all real and reactive power control inputs and let $\hat{u} \in \Re^{m\times 1}$ and $\hat{v} \in \Re^{m\times 1}$ be the vectors consisting of the outputs of the integrator block for each ES controller for channel $u$ and $v$, respectively. Finally, define $q(t) = [a_1 \cos(\omega_1 t), \ldots, a_m \cos(\omega_m t)]^T$ as the vector containing all cosine perturbation signals and $s(t) = [a_1 \sin(\omega_1 t), \ldots, a_m \sin(\omega_m t)]^T$ as the vector containing all sine perturbation signals.

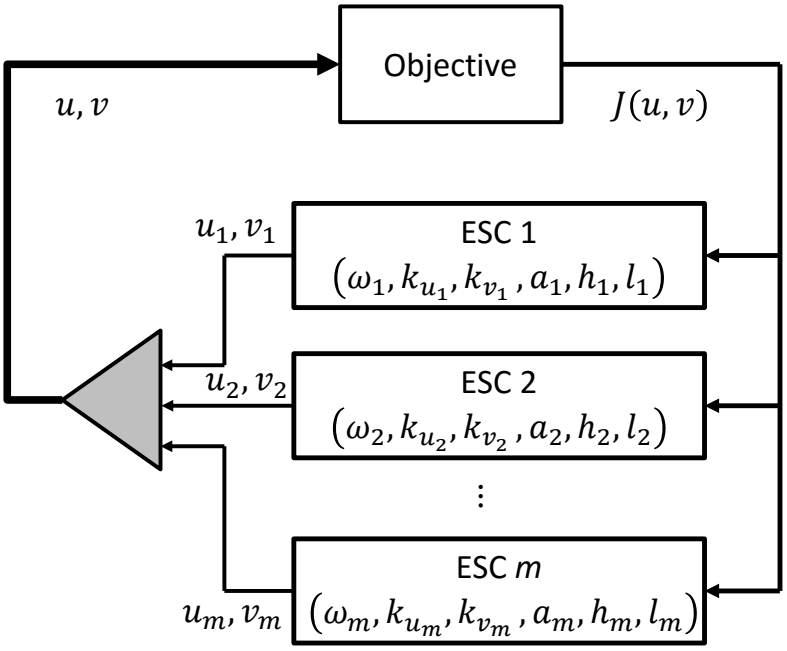



Figure 3.2: Multiple ES controllers in operating in parallel.

In this setting, the vectors of control inputs can be expressed as: $u = \hat{u} + q(t)$ and $v = \hat{v} + s(t)$. For convenience, we define the error systems $\tilde{u} = \hat{u} - u^*$ and $\tilde{v} = \hat{v} - v^*$. Looking now at the $i^{th}$ ES control loop, we have the following nonlinear error dynamics:

$$\dot{e}_i = h_i[\phi(\tilde{u} + q(t), \tilde{v} + s(t)) + J(u^*, v^*) - e_i] \tag{3.3}$$

$$\dot{\xi}_{u_i} = l_i\left[-\xi_{u_i} + \cos(\omega_i t)\left(\phi(\tilde{u} + q(t), \tilde{v} + s(t)) + J(u^*, v^*) - e_i\right)\right] \tag{3.4}$$

$$\dot{\xi}_{v_i} = l_i\left[-\xi_{v_i} + \sin(\omega_i t)\left(\phi(\tilde{u} + q(t), \tilde{v} + s(t)) + J(u^*, v^*) - e_i\right)\right] \tag{3.5}$$

$$\dot{\tilde{u}}_i = -k_{u_i}\xi_{u_i} \tag{3.6}$$

$$\dot{\tilde{v}}_i = -k_{v_i}\xi_{v_i}. \tag{3.7}$$

Let $\tau = \omega_\tau t$ be the lowest common multiple of all time periods in the system such that the entire system is $\tau$-periodic. We may now express the individual probing frequencies as: $\omega_i = \gamma_i \omega_\tau$, where $\gamma_i$ is a positive constant. In the timescale $\tau = \omega_\tau t$, Eqs. (3.3)–(3.7) become:

$$\dot{e}_i = \frac{h_i}{\omega_\tau}\left[\phi(\tilde{u},\tilde{v}) + \nabla_u\phi(\tilde{u},\tilde{v})q(\tau) + \nabla_v\phi(\tilde{u},\tilde{v})s(\tau)\right] + \frac{h_i}{\omega_\tau}\left(J(u^*,v^*) - e_i\right) \tag{3.8}$$

$$\begin{aligned}\dot{\xi}_{u_i} = {} & \frac{l_i}{\omega_\tau}\cos(\gamma_i\tau)\left[\nabla_u\phi(\tilde{u_i},\tilde{v_i})q(\tau) + \nabla_v\phi(\tilde{u_i},\tilde{v_i})s(\tau)\right] \\ & + \frac{l_i}{\omega_\tau}\cos(\gamma_i\tau)\left[\phi(\tilde{u},\tilde{v}) + J(u^*,v^*) - e_i\right] - \frac{l_i}{\omega_\tau}\xi_{u_i}\end{aligned} \tag{3.9}$$

$$\begin{aligned}\dot{\xi}_{v_i} = {} & \frac{l_i}{\omega_\tau}\sin(\gamma_i\tau)\left[\nabla_u\phi(\tilde{u_i},\tilde{v_i})q(\tau) + \nabla_v\phi(\tilde{u_i},\tilde{v_i})s(\tau)\right] \\ & + \frac{l_i}{\omega_\tau}\sin(\gamma_i\tau)\left[\phi(\tilde{u},\tilde{v}) + J(u^*,v^*) - e_i\right] - \frac{l_i}{\omega_\tau}\xi_{v_i}\end{aligned} \tag{3.10}$$

$$\dot{\tilde{u}}_i = -\frac{k_{u_i}}{\omega_\tau}\xi_{u_i} \tag{3.11}$$

$$\dot{\tilde{v}}_i = -\frac{k_{v_i}}{\omega_\tau}\xi_{v_i}, \tag{3.12}$$

where we have approximated $\phi(\tilde{u}+q(t),\tilde{v}+s(t))$ using a Taylor Expansion around $(\tilde{u},\tilde{v})$. As the system of Eqs. (3.8)–(3.12) is now in the form to which averaging is applicable, we integrate over the period 0 to ${}^{\omega_\tau}/_{2\pi}$:

$$\dot{e}_{i,av} = \frac{h_i}{2\pi}[\phi_{av}(\tilde{u}_{av},\tilde{v}_{av}) + J(u^*,v^*) - e_{i,av}] \tag{3.13}$$

$$\dot{\xi}_{u_i,av} = \frac{l_i}{2\pi}\left(-\xi_{u_i,av} + \frac{a_i}{2\gamma_i}\frac{d\phi_{av}}{du_i}(\tilde{u}_{av},\tilde{v}_{av})\right) \tag{3.14}$$

$$\dot{\xi}_{v_i,av} = \frac{l_i}{2\pi}\left(-\xi_{v_i,av} + \frac{a_i}{2\gamma_i}\frac{d\phi_{av}}{dv_i}(\tilde{u}_{av},\tilde{v}_{av})\right) \tag{3.15}$$

$$\dot{\tilde{u}}_{i,av} = -\frac{k_{u_i}}{2\pi}\xi_{u_i,av} \tag{3.16}$$

$$\dot{\tilde{v}}_{i,av} = -\frac{k_{v_i}}{2\pi}\xi_{v_i,av}, \tag{3.17}$$

where the subscript "av" refers to: $\frac{1}{T}\int_0^T(\cdot)d\tau$ and $T = \frac{\omega_\tau}{2\pi}$. Note the dot notation on the derivative terms refer to $\frac{d}{d\tau}$. The averaging process has removed the sinusoidal term in Eq. (3.13) and extracted the averaged gradients of $\phi$ with respect to $u_i$ in Eq. (3.14) and of $\phi$ with respect to $v_i$ in Eq. (3.15). The following properties hold for $\phi_{av}(\tilde{u},\tilde{v})$, $\nabla_u\phi_{av}(\tilde{u},\tilde{v})$, and $\nabla_v\phi_{av}(\tilde{u},\tilde{v})$:

$$\phi_{av}(0,0) = \frac{1}{T}\int_0^T \phi(0,0)d\tau = 0 \tag{3.18}$$

$$\phi_{av}(u,v) > 0, \quad \forall u(t), v(t) \neq 0, \tag{3.19}$$

$$\phi_{av}(u,v) \approx \nabla_u\phi_{av}(u,v)u + \nabla_v\phi_{av}(u,v)v, \tag{3.20}$$

where Eq. (3.20) results from a Taylor Expansion of $\phi_{av}(0,0)$. In light of Eqs. (3.18)–(3.20), the system of Eqs. (3.13)–(3.17) has equilibrium at $(e^{eq}_{i,av}, \xi^{eq}_{u_i,av}, \xi^{eq}_{v_i,av}, \tilde{u}^{eq}_{i,av}, \tilde{v}^{eq}_{i,av}) = (J(u^*,v^*),0,0,0,0)$. At this stage, it is convenient to separate Eqs. (3.13)–(3.17) into two sub-systems: $\dot{e}_{i,av}$ and $(\dot{\xi}^{eq}_{u_i,av}, \dot{\xi}^{eq}_{v_i,av}, \dot{\tilde{u}}^{eq}_{i,av}, \dot{\tilde{v}}^{eq}_{i,av})$, as the latter system does not depend on any states of the former. We continue the analysis with the system:

$$\dot{\xi}_{u_i,av} = \frac{l_i}{2\pi}\left(-\xi_{u_i,av} + \frac{a_i}{2\gamma_i}\frac{d\phi_{av}}{du_i}(\tilde{u}_{av},\tilde{v}_{av})\right) \tag{3.21}$$

$$\dot{\xi}_{v_i,av} = \frac{l_i}{2\pi}\left(-\xi_{v_i,av} + \frac{a_i}{2\gamma_i}\frac{d\phi_{av}}{dv_i}(\tilde{u}_{av},\tilde{v}_{av})\right) \tag{3.22}$$

$$\dot{\tilde{u}}_{i,av} = -\frac{k_{u_i}}{2\pi}\xi_{u_i,av} \tag{3.23}$$

$$\dot{\tilde{v}}_{i,av} = -\frac{k_{v_i}}{2\pi}\xi_{v_i,av}, \tag{3.24}$$

with equilibrium at the origin. In order to show the averaged dynamics for all ES control loops converge to the origin we seek a Lyapunov function $V(\xi_{u,av},\xi_{v,av},\tilde{u}_{av},\tilde{v}_{av}) = \sum_{i=1}^{m} V_i(\xi_{u_i,av},\xi_{v_i,av},\tilde{u}_{i,av},\tilde{v}_{i,av})$, such that $V>0$ and $\dot{V}<0$. It can be verified that choosing $V_i$ such that:

$$V_i = \frac{1}{2}z_i^T A_i z_i + d\int_0^{\tilde{u}_{i,av}} \frac{d\phi_{av}}{du_i}(\tilde{u}_{av}(y),\tilde{v}_{av})dy + d\int_0^{\tilde{v}_{i,av}} \frac{d\phi_{av}}{dv_i}(\tilde{v}_{av},\tilde{v}_{av}(y))dy, \tag{3.25}$$

where $z_i = [\xi_{u_i,av},\xi_{v_i,av},\tilde{u}_{i,av},\tilde{v}_{i,av}]^T$ and

$$A_i = \frac{2\gamma_i}{a_i}\begin{bmatrix} \frac{k_{u_i}}{l_i}d & -c & 0 & 0 \\ -c & \frac{l_i}{k_{u_i}}c & 0 & 0 \\ 0 & 0 & \frac{k_{v_i}}{l_i}d & -c \\ 0 & 0 & -c & \frac{l_i}{k_{v_i}}c \end{bmatrix}, \tag{3.26}$$

with $d>c>0$ yields the desired functions:

$$V(z) = \frac{1}{2}\sum_{i=1}^{m} z_i^T A_i z_i + d\int_0^{\tilde{u}_{av}} \nabla_y\phi_{av}(y,\tilde{v}_{av})dy + d\int_0^{\tilde{v}_{av}} \nabla_y\phi_{av}(\tilde{u}_{av},y)dy \tag{3.27}$$

$$= \frac{1}{2}\sum_{i=1}^{m} z_i^T A_i z_i + d\phi(\tilde{u}_{av},\tilde{v}_{av}) \tag{3.28}$$

$$\dot{V}(z) = -\frac{(d-c)}{2\pi}\sum_{i=1}^{m}\left[\left(\frac{2k_{u_i}\gamma_i}{a_i}\right)\xi_{u_i,av}^2 + \left(\frac{2k_{v_i}\gamma_i}{a_i}\right)\xi_{v_i,av}^2\right] - c\left[\nabla_u\phi_{av}(\tilde{u}_{av},\tilde{v}_{av})\tilde{u}_{av} + \nabla_v\phi_{av}(\tilde{u}_{av},\tilde{v}_{av})\tilde{v}_{av}\right], \tag{3.29}$$

where the integral terms of Eq. (3.27) are the line integral of gradient vectors (which are equal to $\phi_{av}(\tilde{u}_{av},\tilde{v}_{av}) - \phi_{av}(0,0)$), see Eq. (3.28). It is easily verified that Eqs. (3.28) and (3.29) are positive and negative definite respectively, indicating that $V(\xi_{p,av},\xi_{q,av},\tilde{u}_{av},\tilde{v}_{av})$ decreases along the state trajectories of the system (i.e. $(\tilde{u}_{av},\tilde{v}_{av}) \to (u^*,v^*)$). Convergence of the vectors $(u,v)$ to within a neighborhood of $(u^*,v^*)$ is then guaranteed by the proper choice of the ES control parameters and averaging [11], [22].

## 3.3 Problem Formulation

In this section, I introduce a linearized power flow model for balanced radial networks which is subsequently used to construct a piecewise linear objective function that will enable feeder substation real power and voltage target tracking and distribution voltage regulation.

### System Model

Let $T = (H, E)$ denote rooted tree graph representing a transmission system link serving a balanced radial distribution feeder, where $H$ is the set of nodes of the feeder and the transmission link and $E$ is the set of line segments. Nodes are indexed by $i = \infty, 0, 1, \ldots, m$, where $m$ is the order (number of nodes) of the distribution feeder, and node 0 denotes the feeder head (or substation). Immediately upstream of node 0 is an additional node used to represent the transmission system, indexed by $\infty$. We treat node $\infty$ as an infinite bus, decoupling interactions in the downstream distribution system from the rest of the grid. While the transmission voltage may evolve over time, we assume this evolution takes place on a slower timescale than our inverter control action.

For all $i \in H$ let $y_i$ denote the *squared* magnitude of node $i$ voltage. For adjacent nodes $i$ and $j$, the power/voltage relationship is captured by the system:

$$P_i = p_i(y_i) + u_i + \sum_{j:(i,j)\in E} P_j + \frac{r_{ij}}{y_j}\left(P_j^2 + Q_j^2\right) \tag{3.30}$$

$$Q_i = q_i(y_i) + v_i + \sum_{j:(i,j)\in E} Q_j + \frac{x_{ij}}{y_j}\left(P_j^2 + Q_j^2\right) \tag{3.31}$$

$$y_i = y_j + 2r_{ij}P_j + 2x_{ij}Q_j + \frac{r_{ij}^2 + x_{ij}^2}{y_j}\left(P_j^2 + Q_j^2\right)$$
$$\forall j : (i,j) \in E. \tag{3.32}$$

Equations. (3.30)–(3.32) are a reformulation of the *DistFlow* [19] equations. In this formulation, $P_j$ and $Q_j$ represent the real and reactive power that flows into node $j$ from node $i$, over line segment $(i, j)$. The terms $r_{ij}$ and $x_{ij}$ are rectangular components of edge $(i, j)$ electrical impedance. The quantities $u_i$ and $v_i$ represents real and reactive power, respectively, that can either be sourced or consumed by a DER resource. In this convention, positive demand denotes power consumption and negative demand is power injected, or supplied, to the grid. In this system, node $i$ real and reactive power demands, denoted by $p_i(y_i)$ and $q_i(y_i)$ respectively, are voltage dependent and modeled as:

$$p_i(y_i) = p_i\left(a_i^0 + a_i^1 y_i^{\frac{1}{2}} + a_i^2 y_i\right) \tag{3.33}$$

$$q_i(y_i) = q_i\left(a_i^0 + a_i^1 y_i^{\frac{1}{2}} + a_i^2 y_i\right). \tag{3.34}$$

Eqs. (3.30)–(3.32) along with Eqs. (3.33)–(3.34) represent the power flow model that will be used to generate simulations in Section IV.

## Approximate Model

Unfortunately, it is not straightforward to utilize Eqs. (3.30)–(3.34) to construct a convex optimal power flow program as these equalities are nonlinear and nonconvex. While mathematical programs based on this system can be relaxed into a convex form (see [3, 5, 4]), such approaches are not well suited to the problem considered here, as the ES control algorithm is feedback-based and does not allow for the relaxation of the physics of the system.

As such, in this section we study the properties of a system that approximates Eqs. (3.30)–(3.34) for small perturbations around the current operating state, $(u^*, v^*)$. Our interest lies in understanding if the proposed 2D ES control scheme will be able to drive the system to a nearby desired state and keep it there in the presence of small disturbances. Denote $\delta_u$ and $\delta_v$ as small perturbations around $(u^*, v^*)$ such that nearby states are characterized by: $\tilde{u} = u^* + \delta_u$ and $\tilde{v} = v^* + \delta_v$. We define the approximate system as:

$$P_i(\tilde{u}, \tilde{v}) \approx p_i(y_i) + \tilde{u}_i + \sum_{j:(i,j)\in E} P_j(\tilde{u}, \tilde{v}) + r_{ij} l_j(u^*, v^*) \tag{3.35}$$

$$Q_i(\tilde{u}, \tilde{v}) \approx q_i(y_i) + \tilde{v}_i + \sum_{j:(i,j)\in E} Q_j(\tilde{u}, \tilde{v}) + x_{ij} l_j(u^*, v^*) \tag{3.36}$$

$$y_i(\tilde{u}, \tilde{v}) \approx y_j(\tilde{u}, \tilde{v}) + 2r_{ij} P_j(\tilde{u}, \tilde{v}) + 2x_{ij} Q_j(\tilde{u}, \tilde{v}) + \left(r_{ij}^2 + x_{ij}^2\right) l_j(u^*, v^*), \tag{3.37}$$

where

$$l_j(u^*, v^*) = \frac{P_j^2(u^*, v^*) + Q_j^2(u^*, v^*)}{y_j(u^*, v^*)}. \tag{3.38}$$

In the system of (3.35)–(3.38), we are assuming that $\delta_u$ and $\delta_v$ are small enough that the nonlinear terms of Eqs. (3.30)–(3.32) are essentially constant. This model can be thought of as an extension of the *LinDistFlow* approximation of [19] with constant losses (as opposed to no losses). We further approximate nonlinearities in the load model of Eqs. (3.33)–(3.34) via:

$$p_i(y_i) = p_i \left[ a_i^0 + \left( \frac{a_i^1}{2} + a_i^2 \right) y_i \right] \tag{3.39}$$

$$q_i(y_i) = q_i \left[ a_i^0 + \left( \frac{a_i^1}{2} + a_i^2 \right) y_i \right]. \tag{3.40}$$

Note that [3] uses this model to approximate ZIP load behavior. It is easily verified that Eqs. (3.35)–(3.40) are an affine system in the variables $\delta_u$ and $\delta_v$. Thus, we can conclude that near the point $(u^*, v^*)$, the system of Eqs. (3.35)–(3.40) behaves linearly.

## Objective Function Construction

In this section I develop an objective function for an optimal power flow problem, where the goal is to drive substation real power demand and voltage magnitude to track real power and voltage reference signals, denoted by $P_t$ and $y_t$, while regulating system voltages within $\pm 5\%$ of 1 p.u.. Let $\acute{T} \subset T$ represent distribution system portion of $T$ (nodes 0 to $m$), where $\acute{T} = (\acute{H}, \acute{E})$. Without loss of generality, we assume that a DER with four quadrant capability exists at all nodes $\acute{H}$. Denote the vector of all real power control inputs as $u = [u_1, \cdots, u_m]^T$, and the vector of all reactive power control inputs as $v = [v_1, \cdots, v_m]^T$. The problem is defined as:

$$\begin{aligned} \underset{u,v,y_i,Q_i,P_i}{\text{minimize}} \quad & J = \alpha_P |P_0 - P_t| + \alpha_y |y_0 - y_t| \\ \text{subject to} \quad & (3.30) - (3.34), \\ & \underline{y} \leq y_i \leq \overline{y}, \quad i \in \acute{H}, \end{aligned} \tag{3.41}$$

with positive constants $\alpha_P$ and $\alpha_y$ that weight the terms in the objective. An alternative representation of Eq. (3.41) can be obtained through successive substitutions of Eqs. (3.30)–(3.34) into the objective and inequality constraints. This process eliminates all variables $P_i$, $Q_i$, and $y_i$, leaving $u$ and $v$ as the only decision variables. The resulting program is approximated by replacing the inequality constraints with a penalty function in the objective:

$$\underset{u,v}{\text{minimize}} \quad J(u, v), \tag{3.42}$$

where

$$\begin{aligned} J(u,v) = \alpha_P |P_0(u,v) - P_t| + \alpha_y |y_0(u,v) - y_t| \\ + c_y \sum_{i \in \acute{H}} |\underline{y} - y_i(u,v)| + |y_i(u,v) - \overline{y}|, \end{aligned} \tag{3.43}$$

where positive constant, $c_y$, weights the penalty on voltage magnitude constraints. As was discussed in Section 3.3, the power flow model of Eqs. (3.30)–(3.34) is locally approximated by an affine system (3.35)–(3.40) for small perturbations around the present operating state. As such, Eq. (3.43) is approximated by a linear program for small perturbations around the optimizer, and satisfies convexity requirements required for 2D ES control to work. Simulation results in the following section utilize the un-approximated power flow model of Eqs. (3.30)–(3.34) and demonstrate convergence of the ES controllers.

Although the choice of objective function of Eq. (3.43) might seem unusual, simulation experiments with more traditional quadratic-type terms produced results that were less effective in tracking $P_t$ and $y_t$. While the different objectives tested always produced results that would converge, quadratic objectives consistently converged to larger neighborhoods around the tracking signals. I provide an expanded discussion of this phenomena in the Appendix.

## 3.4 Simulation Results

In this section I demonstrate the ability of ES control to enable feeder-head real power and voltage target tracking, while maintaining acceptable system voltages.

A modified IEEE 37 node distribution feeder model, seen in Fig. 3.3, was utilized for simulations [26]. The feeder voltage and power ratings were left unchanged (4.8kV and 2.5MVA), as were line segment configuration assignments (see [26]). However, in order to create a balanced network, all line segments were assumed to be three phase with configurations in Table 3.1. To simulate the connection to the transmission system, an additional node and line segment was added ahead of node 799, with impedance of $0.02 + j0.08\ \Omega$ p.u. (representing the substation transformer and transmission line segment impedance).

Table 3.1: 37 Node Feeder Line Configurations (see [26] for line segment assignments). Note these values are not p.u.. For this experiment, a base value of $Z_{base} = 9.2\Omega$ was utilized.

| Configuration | R $\left(\frac{\Omega}{mi}\right)$ | X $\left(\frac{\Omega}{mi}\right)$ | $\frac{x}{r}$ | $\frac{r}{x}$ |
|---|---|---|---|---|
| 721 | 0.592 | 0.394 | 0.66 | 1.50 |
| 722 | 0.95 | 0.891 | 0.94 | 1.07 |
| 723 | 2.588 | 1.342 | 0.52 | 1.93 |
| 724 | 4.19 | 1.55 | 0.37 | 2.70 |

One minute demand information used in the simulation was obtained from the Pecan St. project [25]. Demand at each node consists of an average of 10 daily load profiles randomly chosen from sites over the period of July 1, 2014 - Aug. 1, 2014. In order to test the performance of the ES approach in scenarios of high renewables penetration, 40% (4 out of 10) of the load profiles used to generate demand at each node came from sites with PV generation. A constant power factor of 0.9 was used to create reactive power demands and voltage-dependent load coefficients for all nodes were: $[a^0, a^1, a^2] = [0.75, 0.05, 0.2]$.

In this simulation, lossless four quadrant-capable PV inverters were placed at nodes: 741, 732, 744, 718, 742, and 724, each controlled by a 2-D ES algorithm. Solar insolation data (which limits the amount of real power available for control) was also generated from the Pecan St. dataset via averaging PV real power output from 10 randomly chosen sites for each controllable inverter. The maximum solar insolation seen at each inverter was selected as the inverter capacity (see Table 3.2). In addition, these nodes were also monitored for voltage regulation within $\pm$ 5% of feeder head voltage. Parameters of individual ES controllers can be found in Table 3.3, and parameters of the objective function were: $\alpha_P = 15$, $\alpha_y = 25$, $c_y = 100$, $\underline{y} = 0.955^2$, and $\bar{y} = 1.045^2$. Note that the voltage threshold values are tighter than $\pm$ 5% to prevent voltages from crossing the 5% limit (had these values been set at $\pm$ 5%, the ES controllers would only take action when the voltage was exceeded.).

Figures 3.4 – 3.9 depict results from a one hour simulation from 13:30 to 14:30 with timesteps of 0.1 seconds with a fixed transmission system voltage of $V_\infty = 1.035$ p.u. The

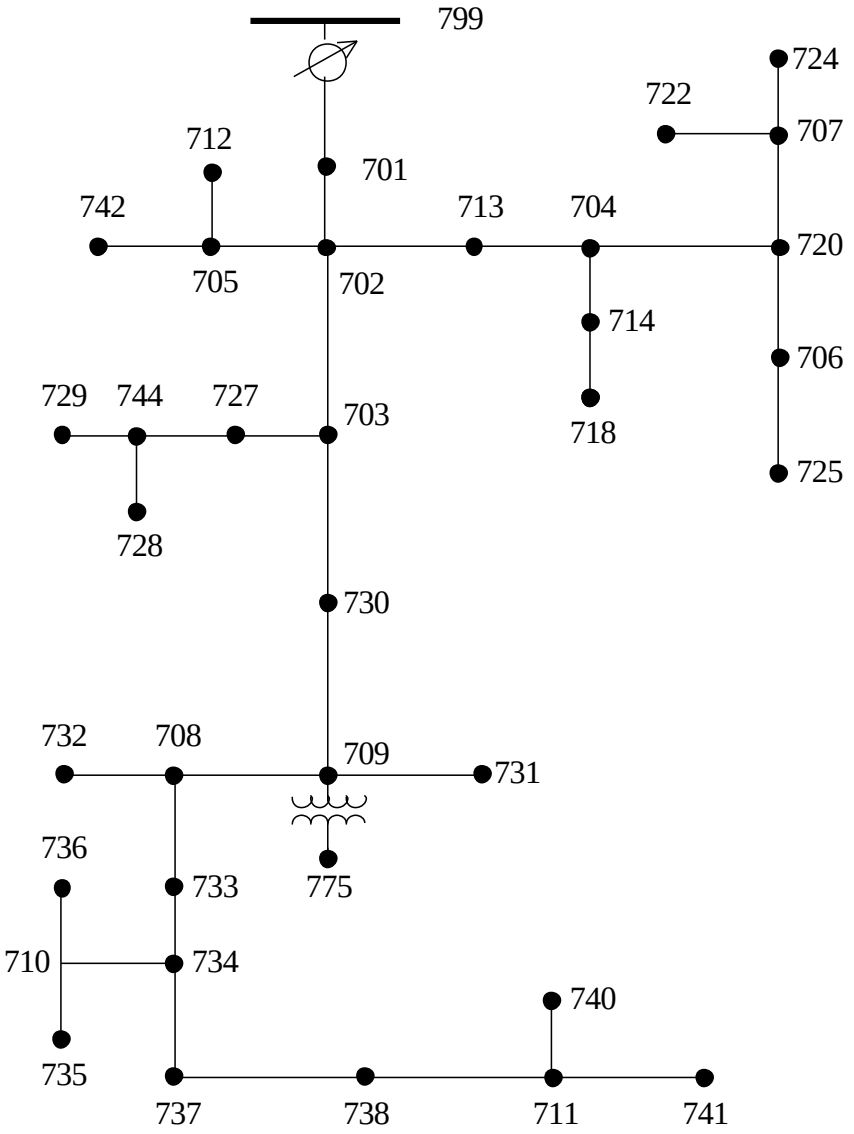



Figure 3.3: IEEE 37 node feeder model.

Table 3.2: Inverter capacities for controllable DER during the simulation. $S_{cap}$ represents the per unit inverter apparent power capacity.

| **Node** | **741** | **732** | **744** | **718** | **742** | **724** |
|---|---|---|---|---|---|---|
| $S_{cap}$ | 0.036 | 0.038 | 0.041 | 0.05 | 0.04 | 0.045 |

Table 3.3: ES simulation parameters for the 37 node feeder experiment.

| **Node** | **711** | **708** | **744** | **718** | **742** | **724** |
|---|---|---|---|---|---|---|
| $f$ (Hz) | 1.9 | $\sqrt{3}$ | 1.8 | $\frac{\sqrt{11}}{2}$ | 2 | 1.59 |
| $h$ ($\frac{rad}{s}$) | 0.0001 | 0.0001 | 0.0001 | 0.0001 | 0.0001 | 0.0001 |
| $l$ ($\frac{rad}{s}$) | 0.05 | 0.05 | 0.05 | 0.05 | 0.05 | 0.05 |
| $k_u$ | -0.5 | -0.5 | -0.5 | -0.5 | -0.5 | -0.5 |
| $k_v$ | -0.05 | -0.05 | -0.05 | -0.05 | -0.05 | -0.05 |
| $a$ (p.u.) | 0.0005 | 0.0005 | 0.0005 | 0.0005 | 0.0005 | 0.0005 |

real power target, $P_t$ was generated from a scaled version of a PJM regulation self test signal [27], and the voltage reference signal, $y_t$, was fixed to $1.0^2$ for the duration of the simulation. As the results show, the 2-D ES controllers successfully track the real power and voltage targets at the substation and drive system voltages to within acceptable ranges. For comparison, Figs. 3.4 - 3.5 also depict a "Unity Power Factor" case where controllable inverters are *not* managed by 2D-ES algorithms and, instead, output only real power (i.e. no reactive power control). "Base Case" depicts the feeder behavior in the absence of any control entirely. It should be noted that, in this situation, in order to track simultaneously both real power and voltage reference signals, ES controllers needed to curtail PV real power output. It should also be noted that the physical devices that provide real and reactive power control capabilities need not be PV inverters. DER with the ability to continuously modulate power outputs (such as inverters associated with battery storage systems) would also suffice.

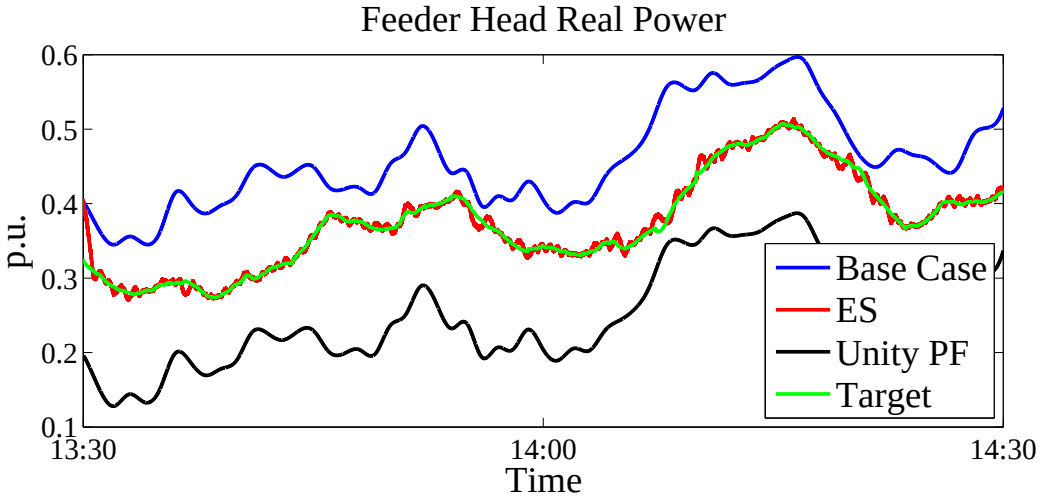



Figure 3.4: Feeder head (substation) real power.

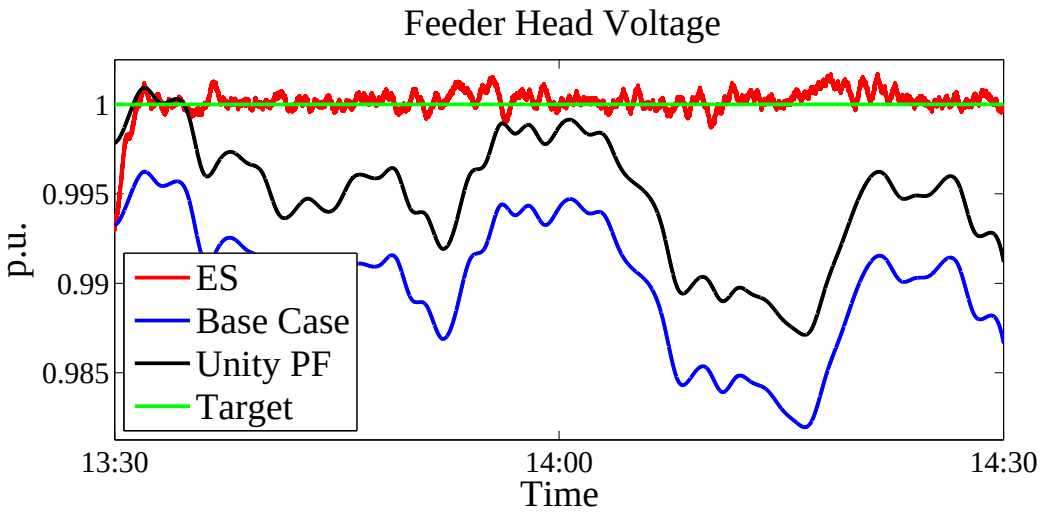



Figure 3.5: Feeder head (substation) voltage.

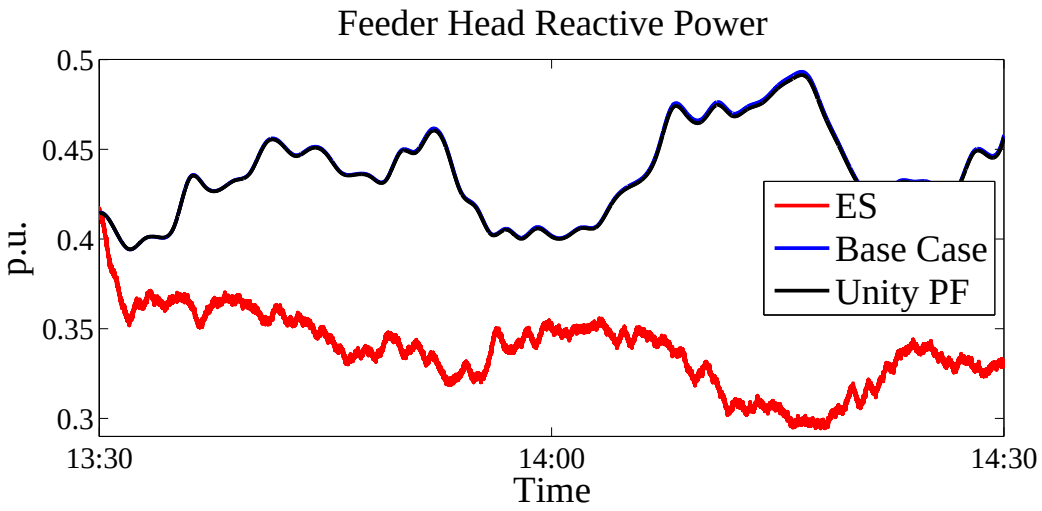



Figure 3.6: Feeder head (substation) reactive power.

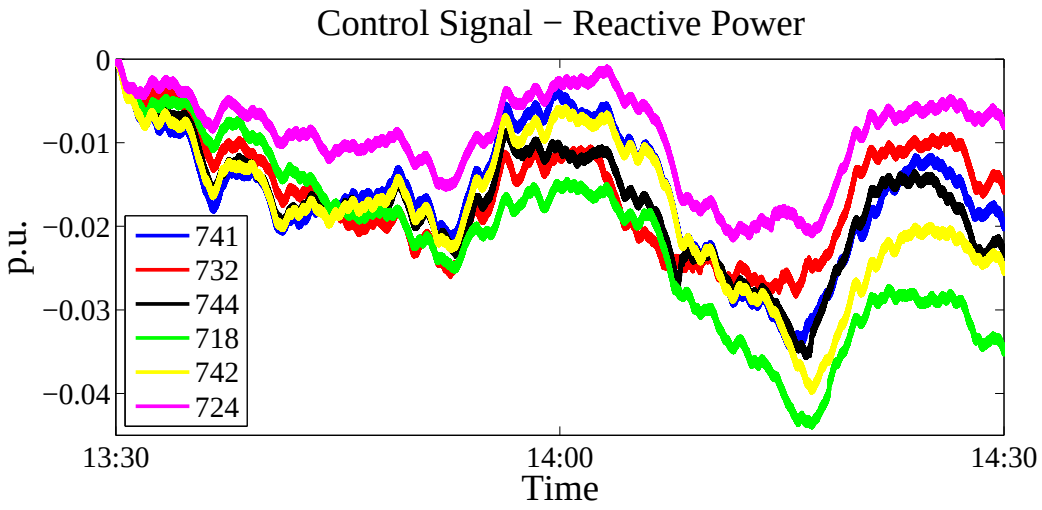



Figure 3.7: Reactive power output of controllable DER.

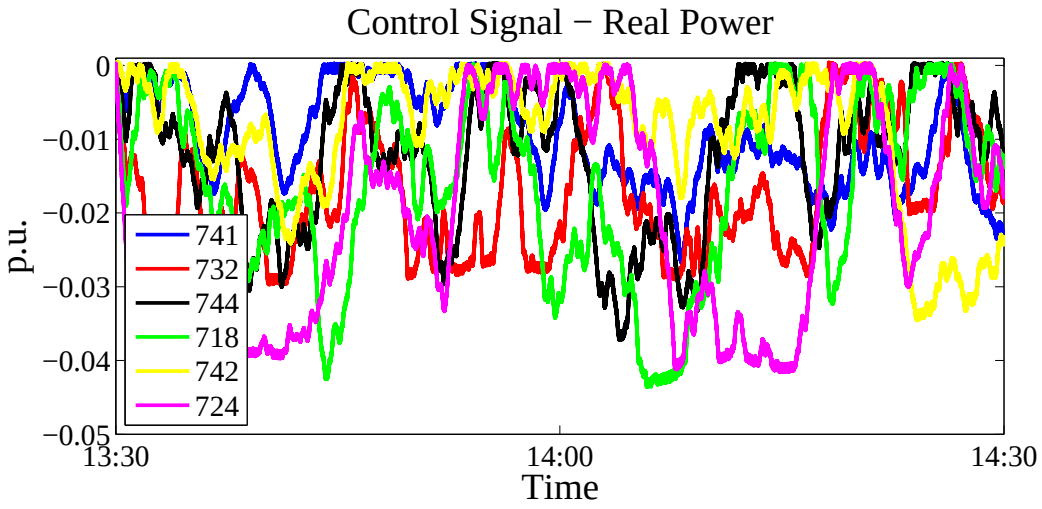



Figure 3.8: Real power output of controllable DER.

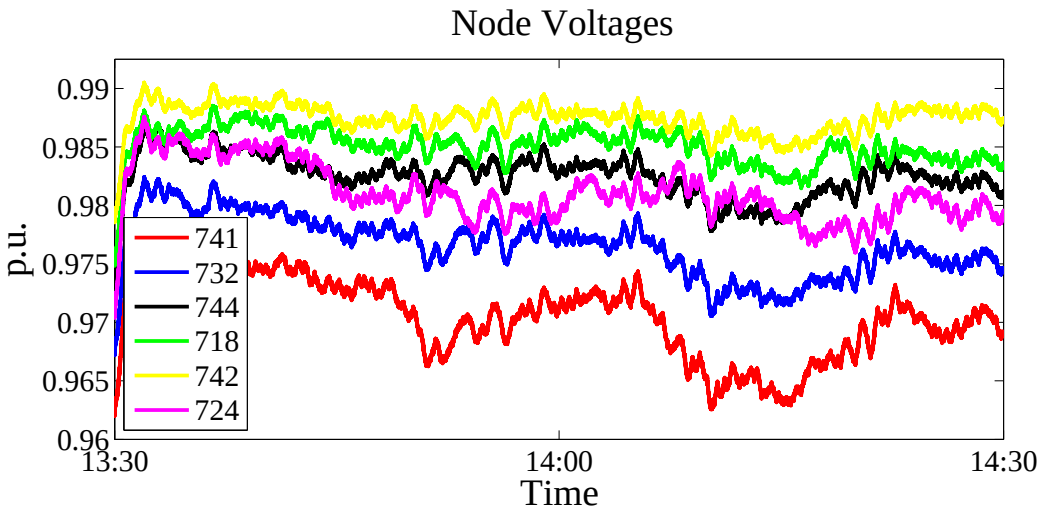



Figure 3.9: Voltage profiles for regulated nodes during the simulation.

## 3.5 Concluding Remarks

This work considered distributed model-free optimization of distribution systems using four-quadrant-capable DER. A 2 dimensional *Extremum Seeking* control algorithm was employed to manage both the real power and reactive power output of controllable resources. While in Chapter 2, I utilized a sinusoidal probe to control only reactive power, in this work I used the orthogonal sinusoid of the same frequency to allow for *simultaneous* control of inverter real and reactive power. In simulations I demonstrated distribution feeder substation real power and voltage reference tracking using PV systems managed by 2-D ES controllers, which essentially allows the distribution feeder to emulate a (P,V) bus when viewed from the perspective of the transmission system operator.

Although Section 3.4 demonstrated PV systems providing real and reactive power support, the ES control approach could be utilized by advanced power inverters associated with other types of DER, such as electric vehicle and battery storage systems. Such DER have the potential to modulate their power outputs on timescales suitable for ES control and can either provide their own independent probes and/or share probing responsibilities with neighbors. However, it is also possible to extend the approach to support equipment incapable of actuating on timescales required for ES probing, such as demand response assets. To do so, it would be necessary to utilize the probing signal from another piece of hardware such as nearby DER capable of probing, or a dedicated probing resource.

With this work, I have shown that model-free and distributed control algorithms can optimally provide regulation services to the bulk grid while maintaining internal voltage stability in the distribution system. Moving forward, I intend to explore the use of ES control to manage four-quadrant-capable DER in *unbalanced* distribution systems, and incorporate binary and integer-type controllable resources (such as demand response assets and legacy voltage regulation equipment) into this control paradigm. As was discussed in Section 2.5, an extension of ES to manage unbalanced power flow is considerably more complex than the balanced case, and it is not expected to be able to derive sufficient conditions similar to Theorem 1. However, one may study approximate system behavior using suitable linearized power flow models. Though not considered explicitly in this dissertation, Chapter 4 lays the groundwork for 3-phase ES through deriving such a linearization.

# Chapter 4

# Linear OPF Formulation for Unbalanced Systems

Optimization of distributed power assets is a powerful tool that has the potential to assist utility efforts to ensure customer voltages are within pre-defined tolerances and to improve distribution system operations. While convex relaxations of Optimal Power Flow (OPF) problems have been proposed for both balanced and unbalanced networks, these approaches do not provide universal convexity guarantees and scale inefficiently as network size and the number of constraints increase. In balanced networks, a linearized model of power flow, the LinDistFlow model, has been successfully employed to solve approximate OPF problems quickly and with high degrees of accuracy. In this work, an extension of the LinDistFlow model is proposed for unbalanced distribution systems, and is subsequently used to formulate an approximate unbalanced OPF problem that uses VAR assets for voltage balancing and regulation. Simulation results on the IEEE 13 node test feeder demonstrate the ability of the unbalanced LinDistFlow model to perform voltage regulation and balance system voltages.

## 4.1 Preface

Coordination of a diverse set of Distributed Energy Resources (DER) presents many challenges to utility operators, who strive to ensure power of sufficient quality and quantity is available to retail customers at least cost. Such assets can vary in size from residential rooftop PV units to larger PV arrays and, perhaps, battery storage systems located at residential, commercials and industrial sites. As has been experienced in Hawaii [1], the negative impact of high levels of distributed PV under current interconnection standards is significant, and has led to financial impacts to both consumers and the utility. However, distributed generation resources could, under the correct operational control scenarios, provide numerous benefits to the grid, including voltage support and VAR compensation.

A variety of strategies for the management of DER presently exist for *balanced* distribution system models. Turitsyn et al. [6] considered a suite of distributed control strategies for reactive power compensation using four quadrant inverters. The work of [7] studies distributed voltage regulation in the absence of communication, relying on locally obtained information. Their results extend to optimize the cost of reactive power and are based on linearized power flow approximations. In [8], a two-stage control architecture for voltage regulation is considered where distributed controllers inject power based on local sensitivity measurements. The authors of [9] study local voltage reference tracking with integral-type controllers, based on local voltage measurements. The authors of [3] address voltage regulation and loss minimization through solving an Optimal Power Flow (OPF) problem, and address convexity issues using second order cone relaxations. The work of [4] also considers an OPF approach for voltage regulation in distribution networks by framing the decision-making process a semidefinite program. The authors provide conditions under which the semidefinite relaxation of the nonconvex power flow problem is tight in balanced circuits. It is worth noting that many of the aforementioned approaches can be traced back to the seminal work of [19], that introduced nonlinear and linear-approximated recursive branch power flow models.

Approaches to coordinate DER in *unbalanced* distribution systems are much less prevalent. Perhaps the best known efforts have been put forth by the authors of [5], who consider semidefinite relaxations for OPF problems in unbalanced systems, but do not provide conditions under which optimality is guaranteed. In addition to inefficient scaling as the problem size increases, the work of [28] points out that it becomes more difficult to find a tight relaxation as the ratio of constraints to network buses increases. A likely reason that more strategies focusing on coordination of DER in unbalanced systems do not exist is the lack of suitable linear models that approximate three phase power flow.

This work attempts to fill that void by proposing a linearized unbalanced power flow model that can be viewed as an extension of the *LinDistFlow* [19] linear approximation for balanced systems. While additional complexities due to cross-phase interactions increase the degree of nonlinearity of unbalanced power flow, this new approximation derived in this work is made possible by assuming that the ratio of voltage phasors are constant and equal to $1 \pm 120°$. Using this new linear model, I construct an OPF formulation that dispatches

reactive power resources from controllable power electronic inverters to perform voltage balancing and regulation. Voltage balancing is an important objective to reduce neutral current flow in wye connected circuits, simplify the operation of voltage regulation equipment, and, for the efficient operation of three phase induction motors (which are commonly derated if voltage imbalance is too high). My results show that OPF formulations that utilize the linearized three phase *LinDistFlow* model result in a dispatch of inverter VAR resources that successfully drives system voltages into acceptable regimes and simultaneously balances voltages by reducing magnitude differences between phases.

This work is organized as follows. A model of nonlinear three phase unbalanced power flow is introduced in Section 4.2. This model, used in simulations later in the chapter, is also used in the derivation of the linear approximation for three phase power flow in Section 4.3. Section 4.4 formulates an OPF to perform voltage regulation and balancing, and discusses results from simulation. Finally, concluding remarks are provided in Section 4.5.

# Nomenclature

$V_{\phi,k}$ : Voltage phasor at node $k$ on phase $\phi$
$\mathbb{V}_k$ : Vector of voltage phasors at node $k$
$y_{\phi,k}$ : Square magnitude of voltage at node $k$ on phase $\phi$
$\mathbb{Y}_k$ : Vector of square magnitudes of voltage at node $k$
$Z_{\phi\phi,jk}$ : Impedance of segment $(j,k)$ on phase $\phi$
$Z_{\phi\psi,jk}$ : Impedance of segment $(j,k)$ between phases $(\phi,\psi)$
$\mathbb{Z}_{jk}$ : Impedance matrix of line segment $(j,k)$
$I_{\phi,k}$ : Current phasor entering node $k$ on phase $\phi$
$\mathbb{I}_k$ : Vector of current phasors entering node $k$
$i_{\phi,k}$ : Load current of phase $\phi$ at node $k$
$\mathbf{i}_k$ : Vector of load currents at node $k$
$S_{\phi,k}$ : Complex power entering node $k$ on phase $\phi$
$\mathbb{S}_k$ : Vector of complex powers entering node $k$
$s_{\phi,k}$ : Complex load on phase $\phi$ at node $k$
$\mathbf{s}_k$ : Vector of complex loads at node $k$
$u_{\phi,k}$ : Inverter VAR dispatch on phase $\phi$ at node $k$

## 4.2 Preliminaries

Let $T = (H, E)$ denote rooted tree graph representing a balanced radial distribution feeder, where $H$ is the set of nodes of the feeder and the transmission link and $E$ is the set of line segments. Nodes are indexed by $i = 0, 1, \ldots, m$, where $m$ is the order (number of nodes) of the distribution feeder, and node 0 denotes the feeder head (or substation). We treat node 0 as an infinite bus, decoupling interactions in the downstream distribution system from the rest of the grid. While the substation voltage may evolve over time, we assume this evolution takes place independently of our inverter control action. For adjacent nodes $j$ and $k$, the current/voltage relationship is captured by KVL and KCL:

$$\begin{bmatrix} V_a \\ V_b \\ V_c \end{bmatrix}_j = \begin{bmatrix} V_a \\ V_b \\ V_c \end{bmatrix}_k + \begin{bmatrix} Z_{aa} & Z_{ab} & Z_{ac} \\ Z_{ba} & Z_{bb} & Z_{bc} \\ Z_{ca} & Z_{cb} & Z_{cc} \end{bmatrix}_{jk} \begin{bmatrix} I_a \\ I_b \\ I_c \end{bmatrix}_k \tag{4.1}$$

$$\begin{bmatrix} I_a \\ I_b \\ I_c \end{bmatrix}_j = \begin{bmatrix} i_a \\ i_b \\ i_c \end{bmatrix}_j + \sum_{k:(j,k)\in E} \begin{bmatrix} I_a \\ I_b \\ I_c \end{bmatrix}_k, \tag{4.2}$$

where $i_a$ denotes phase $a$ load current, and $Z_{aa}$ and $Z_{ab}$ are the self impedance for phase $a$ and mutual impedance between phases $a$ and $b$, etc.. We assume that each node serves a complex load in each phase, $s_{\phi,k} = V_{\phi,k} i^*_{\phi,k}$ whose real and reactive power components are given by (4.3) and (4.4), respectively.

$$p_{\phi,k}(V_{\phi,k}) = p_{\phi,k}\left(a^0_{\phi,k} + a^1_{\phi,k}\left|V_{\phi,k}\right|^2\right) \tag{4.3}$$

$$q_{\phi,k}(V_{\phi,k}) = q_{\phi,k}\left(a^0_{\phi,k} + a^1_{\phi,k}\left|V_{\phi,k}\right|^2\right) + u_{\phi,k} \tag{4.4}$$

where $a^0_k + a^1_k = 1$ and are, for simplicity, assumed constant across all phases at each node. $u_{\phi,k}$ is the reactive power that can be sourced or consumed from a VAR resource on phase $\phi$ at node $k$. In our convention, positive demand denotes power consumption and negative demand is power injected, or supplied, to the grid. Equations (4.1)–(4.4) represent the power flow model that will be used to generate simulations in Section 4.4.

## 4.3 Derivation of Linearized Model

In this section, I derive a linear approximation of three phase power flow. This model can be thought of as an extension of the *LinDistFlow* model to unbalanced circuits. Consider two adjacent nodes of the distribution feeder, $(j,k) \in H$. We begin by expressing (4.1)–(4.2) in vector form:

$$\mathbb{V}_j = \mathbb{V}_k + \mathbb{Z}_k \mathbb{I}_k \tag{4.5}$$

$$\mathbb{I}_j = \mathbf{i}_j + \sum_{k:(j,k)\in E} \mathbb{I}_k. \tag{4.6}$$

We now right multiply each side of (4.5) by its complex conjugate and right multiply both sides of (4.6) by $\mathbb{V}_j^*$ and take the complex conjugate, resulting in:

$$\begin{aligned}\mathbb{V}_j \mathbb{V}_j^* &= \mathbb{V}_k \mathbb{V}_k^* + \mathbb{Z}_k \mathbb{I}_k \mathbb{V}_k^* + \mathbb{V}_k \mathbb{I}_k^* \mathbb{Z}_k^* + \mathbb{Z}_k \mathbb{I}_k \mathbb{I}_k^* \mathbb{Z}_k^* \\ &= \mathbb{V}_k \mathbb{V}_k^* + 2\Re\left\{\mathbb{V}_k \mathbb{I}_k^* \mathbb{Z}_k^*\right\} + \mathbb{Z}_k \mathbb{I}_k \mathbb{I}_k^* \mathbb{Z}_k^*, \end{aligned} \tag{4.7}$$

$$\mathbb{V}_j \mathbb{I}_j^* = \mathbb{V}_j \mathbf{i}_j^* + \sum_{k:(j,k)\in E} \left(\mathbb{V}_k + \mathbb{Z}_k \mathbb{I}_k\right) \mathbb{I}_k^*. \tag{4.8}$$

Similar to the derivation of the *LinDistFlow* system, we neglect loss terms in (4.7)–(4.8), which yields:

$$\mathbb{V}_j \mathbb{V}_j^* \approx \mathbb{V}_k \mathbb{V}_k^* + 2\Re\left\{\mathbb{V}_k \mathbb{I}_k^* \mathbb{Z}_k^*\right\} \tag{4.9}$$

$$\mathbb{V}_j \mathbb{I}_j^* \approx \mathbb{V}_j \mathbf{i}_j^* + \sum_{k:(j,k)\in E} \mathbb{V}_k \mathbb{I}_k^*. \tag{4.10}$$

where (4.9)–(4.10) are $3 \times 3$ matrix equations. Focusing our attention first on (4.10), we apply the power equation $S_{\phi,k} = V_{\phi,k} I_{\phi,k}^*$ to the diagonal elements and collect these into the vector equation:

$$\mathbb{S}_j \approx \mathbf{s}_j + \sum_{k:(j,k)\in E} \mathbb{S}_k. \tag{4.11}$$

Returning attention to (4.9), we expand $\mathbb{I}_k$ according to $S_{\phi,k} = V_{\phi,k} I_{\phi,k}^*$, resulting in:

$$\mathbb{V}_j \mathbb{V}_j^* \approx \mathbb{V}_k \mathbb{V}_k^* + 2\Re\left\{\mathbb{V}_k \begin{bmatrix} S_a V_a^{-1} & S_b V_b^{-1} & S_c V_c^{-1} \end{bmatrix}_k \mathbb{Z}_{jk}^*\right\} \tag{4.12}$$

which is equivalent to:

$$\mathbb{V}_j\mathbb{V}_j^* \approx \mathbb{V}_k\mathbb{V}_k^* + 2\Re\left\{\begin{bmatrix} S_a & V_aS_bV_b^{-1} & V_aS_cV_c^{-1} \\ V_bS_aV_a^{-1} & S_b & V_bS_cV_c^{-1} \\ V_cS_aV_a^{-1} & V_cS_bV_b^{-1} & S_c \end{bmatrix}_k \mathbb{Z}_{jk}^*\right\} \quad . \tag{4.13}$$

Note that even after neglecting the loss terms, (4.13) is still nonlinear. To further simplify the system, we adopt an approximation that assumes the ratio of voltage phasors are constant:

$$V_{a,k}V_{b,k}^{-1} \approx \alpha \quad V_{b,k}V_{c,k}^{-1} \approx \alpha \quad V_{a,k}V_{c,k}^{-1} \approx \alpha^2 \tag{4.14}$$

where

$$\alpha = 1\angle 120^\circ = \frac{-1+j\sqrt{3}}{2}, \quad \alpha^2 = 1\angle 240^\circ = -\frac{1+j\sqrt{3}}{2}. \tag{4.15}$$

The simplification of the quotient of the voltage phasors according to (4.14)–(4.15) transforms (4.13) into:

$$\mathbb{V}_j\mathbb{V}_j^* \approx \mathbb{V}_k\mathbb{V}_k^* + 2\Re\left\{\begin{bmatrix} S_a & \alpha S_b & \alpha^2 S_c \\ \alpha^2 S_a & S_b & \alpha S_c \\ \alpha S_a & \alpha^2 S_b & S_c \end{bmatrix}_k \mathbb{Z}_{jk}^*\right\} \tag{4.16}$$

Although (4.16) is a $3 \times 3$ matrix equation, we are intertested only in the diagonal elements, which we gather and place into $3 \times 1$ vectors resulting in (4.17):

$$\mathbb{Y}_j \approx \mathbb{Y}_k + 2\Re\left\{\begin{bmatrix} Z_{aa,jk}^* S_{a,k} + \alpha Z_{ab,jk}^* S_{b,k} + \alpha^2 Z_{ac,jk}^* S_{c,k} \\ \alpha^2 Z_{ba,jk}^* S_{a,k} + Z_{bb,jk}^* S_{b,k} + \alpha Z_{bc,jk}^* S_{c,k} \\ \alpha Z_{ca,jk}^* S_{a,k} + \alpha^2 Z_{cb,jk}^* S_{b,k} + Z_{cc,jk}^* S_{c,k} \end{bmatrix}\right\}, \tag{4.17}$$

where we have defined the vector of the square of voltage magnitudes in phases $a, b, c$ as $\mathbb{Y}_k = \begin{bmatrix} y_a & y_b & y_c \end{bmatrix}_k^T$. The $3 \times 1$ vector inside the $\Re$ operator can be broken up into a $3 \times 3$ matrix of impedances for line segment $(j, k)$ and a $3 \times 1$ vector of node $k$ power injections, as is shown in (4.18).

$$\mathbb{Y}_j \approx \mathbb{Y}_k + 2\Re\left\{\begin{bmatrix} Z_{aa}^* & \alpha Z_{ab}^* & \alpha^2 Z_{ac}^* \\ \alpha^2 Z_{ba}^* & Z_{bb}^* & \alpha Z_{bc}^* \\ \alpha Z_{ca}^* & \alpha^2 Z_{cb}^* & Z_{cc}^* \end{bmatrix}_{jk} \begin{bmatrix} S_a \\ S_b \\ S_c \end{bmatrix}_k\right\} \tag{4.18}$$

Viewed in this form, the approximation to the ratio of voltage phasors essentially introduces $\pm 120^\circ$ rotations of the cross-phase impedances. Expanding the impedance matrix entries as $Z_{\phi\psi,k} = r_{\phi\psi,k} + jx_{\phi\psi,k}$, the complex power as $S_{\phi,k} = P_{\phi,k} + jQ_{\phi,k}$, and using

the definition of $\alpha$, it can be shown that (4.18) simplifies into the following linear matrix equation:

$$\mathbb{Y}_j \approx \mathbb{Y}_k - \mathbb{M}_{jk}^P \mathbb{P}_k - \mathbb{M}_{jk}^Q \mathbb{Q}_k \tag{4.19}$$

where

$$\mathbb{M}_{jk}^P = \begin{bmatrix} -2r_{aa} & r_{ab} - \sqrt{3}x_{ab} & r_{ac} + \sqrt{3}x_{ac} \\ r_{ba} + \sqrt{3}x_{ba} & -2r_{bb} & r_{bc} - \sqrt{3}x_{bc} \\ r_{ca} - \sqrt{3}x_{ca} & r_{cb} + \sqrt{3}x_{cb} & -2r_{cc} \end{bmatrix}_{jk} \tag{4.20}$$

$$\mathbb{M}_{jk}^Q = \begin{bmatrix} -2x_{aa} & x_{ab} + \sqrt{3}r_{ab} & x_{ac} - \sqrt{3}r_{ac} \\ x_{ba} - \sqrt{3}r_{ba} & -2x_{bb} & x_{bc} + \sqrt{3}r_{bc} \\ x_{ca} + \sqrt{3}r_{ca} & x_{cb} - \sqrt{3}r_{cb} & -2x_{cc} \end{bmatrix}_{jk}. \tag{4.21}$$

We now restate (4.11) for completeness:

$$\mathbb{S}_j \approx \mathbf{s}_j + \sum_{k:(j,k)\in E} \mathbb{S}_k \tag{4.22}$$

Equations (4.19)–(4.22) represent a linearized model of unbalanced distribution power flow that maps node $k$ real and reactive power injections into squared voltage magnitude differences. As the system shows, power contribution in all three phases collectively influence each phase's squared voltage magnitude difference. It is easily verified that a reduction to a single phase network results in the *LinDistFlow* model discussed in [19].

## 4.4 Simulation Results

In this section, I incorporate the linearized three phase power flow model into an OPF program. The goal of the optimization is to control inverter VAR resources in a distribution system to regulate and balance system voltages. The problem is defined as:

$$\begin{aligned} \underset{u,y_i,Q_i,P_i}{\text{minimize}} \quad & \sum_{i\in H}\left[\sum_{\substack{\phi,\psi\in\{a,b,c\}\\ \phi\neq\psi}}(y_{\phi,i}-y_{\psi,i})^2\right]+\rho u_{\phi,i}^2 \\ \text{subject to} \quad & (4.19)-(4.22), \\ & \underline{y}\leq y_i\leq \overline{y}, \quad \forall i\in H, \end{aligned} \tag{4.23}$$

where $\rho$ is positive (0.5 in simulations) and $\underline{y}$ and $\overline{y}$ represent upper and lower bounds on voltage magnitude (which are fixed to $0.95^2$ and $1.05^2$), respectively. The first term in the objective function is the sum of squared Euclidean distances of squared voltage magnitude differences across phases at each node. The second term penalizes the use of inverter VAR resources.

The OPF is tested on the IEEE 13 test node distribution feeder [26], seen in Fig. 4.1. This simulation neglects the presence of the voltage regulator between nodes 650 and 632, the transformer between nodes 633 and 634, the switch (assumed closed) between nodes 671 and 692, and capacitors at nodes 675 and 611. Constant power and constant impedance load fractions were assigned as $a_i^0 = 0.85$ and $a_i^1 = 0.15$.

Feeder configurations, per-length line segment impedances, and line segment lengths can be found in [26]. All line segment impedances were increased by a factor of 1.25. Spot loads (also found in [26]) were assigned to nodes according to Table 4.1. Distributed loads were neglected. For the simulation, feeder power and voltage base values were chosen as the power rating and secondary voltage of the substation transformer, 500kVA and 4.16kV respectively. Additionally, feeder head voltage was fixed to 1 p.u.. Controllable three phase inverter resources were placed at nodes 632, 675, 680, and 684. These resources were purposefully left unconstrained to test the effectiveness of the OPF, with the ability to source or sink arbitrary amounts of reactive power.

Simulation results are presented in Figs. 4.2 - 4.8 and in Table 4.2. Voltage profiles for the base scenario (where inverter VAR resources are not utilized) and control scenario (inverter VAR resources are determined by the OPF of (4.23)) can be seen in Figs. 4.2 - 4.4. As the figures show, in the control case, the voltage magnitudes of phase $a$ are kept almost constant with the base case. The voltage magnitudes of phase $b$ are decreased, and of $c$ are increased, to achieve greater voltage magnitude balance. Additionally, the voltages of phase $c$, originally in violation of the lower voltage bound, are now within the acceptable $\pm 5\%$ threshold. It should be noted that the rise in voltage magnitude for the base scenario from node 632 to node 671 reconciles with power-flow simulation results in [26] and is likely due to the fact that off diagonal components of (4.20)-(4.21) have *opposite* signs of the

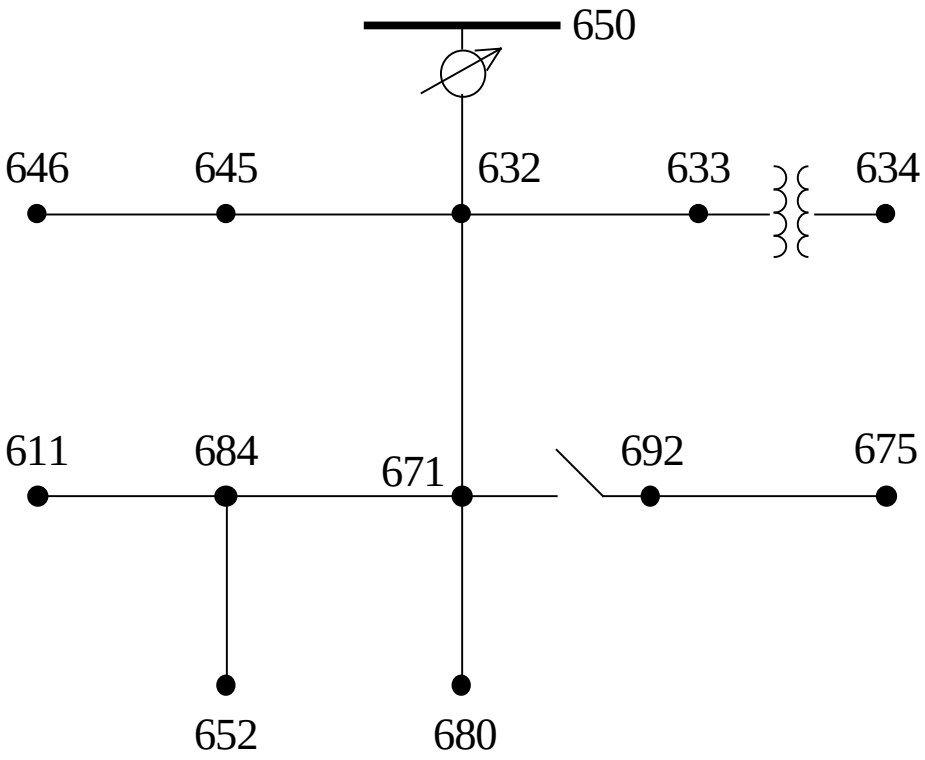



Figure 4.1: IEEE 13 node feeder model.

diagonal components, indicating that large voltage drops in some phases actually contribute to voltage *rises* in other phases.

Voltage magnitudes for all phases at each node with and without control action can be seen in Figs. 4.5 and 4.6, respectively. As the figures show, the voltage magnitudes are much closer together when inverter reactive power is dispatched according to the results of the OPF of (4.23).

Figure 4.7 evaluates the first term of objective function of (4.23) for all nodes with and without control action. The results show that the objective function value (which measures the Euclidean distance between squared voltage magnitudes) decreases at all nodes following control action with the exception of node 646, which increases very slightly.

Optimal inverter control output is shown in Fig. 4.8 and listed in Table 4.2. As the figure shows, to balance the system, inverters at node 675 and 632 actually *consume* VARs. This effect is believed to attributed the fact that phase voltages at these nodes are increasing compared to voltages in the remaining phases.

Control action reduced feeder head real power slightly, from 0.660 p.u. to 0.659 p.u. and feeder head reactive power more significantly, from 0.425 p.u. to 0.383 p.u.

Table 4.1: Spot loads of the 13 node feeder.

| | Phase | | |
|---|---|---|---|
| Node | $a$ [pu] | $b$ [pu] | $c$ [pu] |
| 650 | 0 | 0 | 0 |
| 632 | 0 | 0 | 0 |
| 633 | 0 | 0 | 0 |
| 634 | 0.032 + j 0.022 | 0.024 + j 0.018 | 0.024 + j 0.018 |
| 645 | – | 0.034 + j 0.025 | 0 |
| 646 | – | 0.046 + j 0.0264 | 0 |
| 671 | 0.077 + j 0.044 | 0.077 + j 0.044 | 0.077 + j 0.044 |
| 692 | 0 | 0 | 0.034 + j 0.0302 |
| 675 | 0.097 + j 0.038 | 0.0136 + j 0.012 | 0.058 + j 0.0424 |
| 680 | 0 | 0 | 0 |
| 684 | 0 | – | 0 |
| 652 | 0.0256 + j 0.0172 | – | – |
| 611 | – | – | 0.034 + j 0.0106 |
| Total | 0.2316 + j 0.1212 | 0.1946 + j 0.1254 | 0.227 + j 0.1506 |

Table 4.2: Optimal reactive power output of controllers.

| | Phase | | |
|---|---|---|---|
| Node | $a$ [pu] | $b$ [pu] | $c$ [pu] |
| 632 | -0.0081 | -0.0346 | 0.0437 |
| 675 | 0.005 | 0.0522 | -0.058 |
| 680 | 0.003 | 0.0011 | -0.0038 |
| 684 | -0.0003 | – | -0.0389 |
| Total | -0.0003 | 0.0187 | -0.057 |

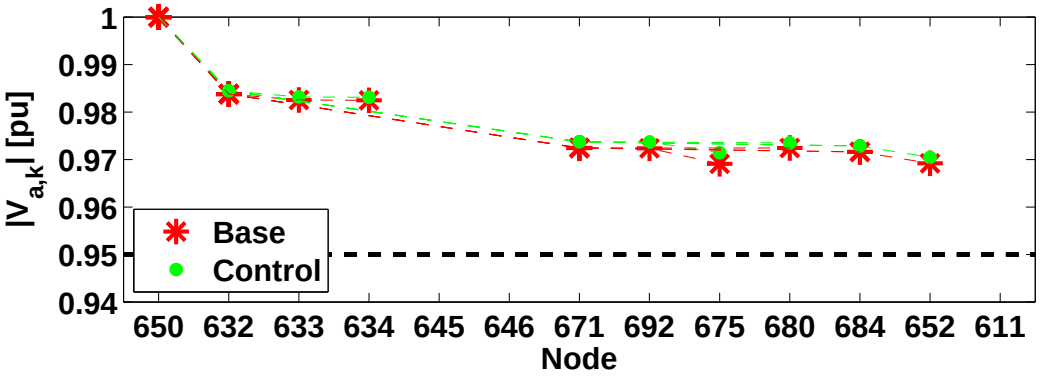



Figure 4.2: Phase $a$ voltage magnitudes for base and control scenarios plotted individually. Dashed lines represent line segments between nodes.

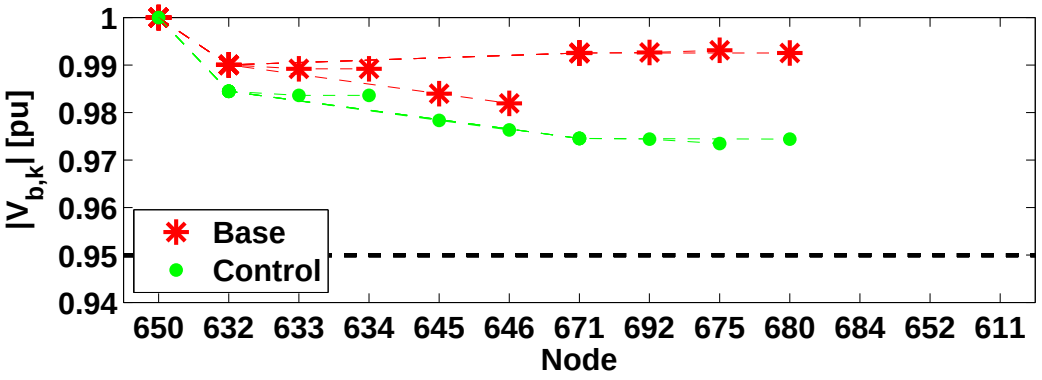



Figure 4.3: Phase $b$ voltage magnitudes for base and control scenarios plotted individually. Dashed lines represent line segments between nodes.

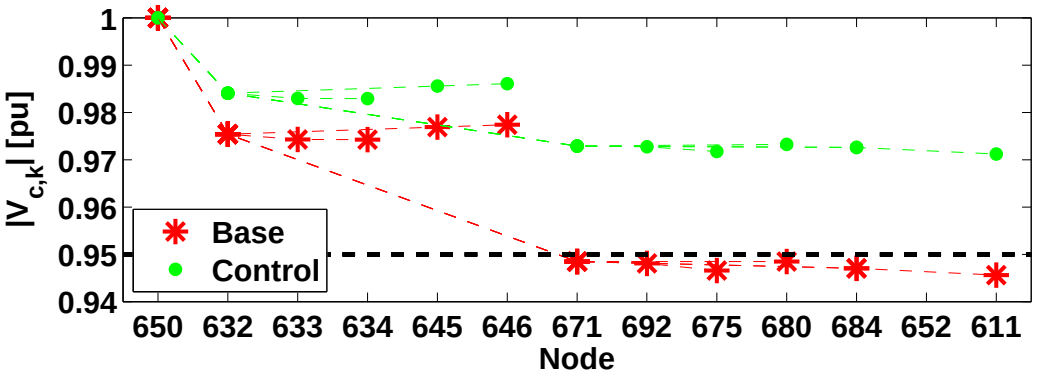



Figure 4.4: Phase $c$ voltage magnitudes for base and control scenarios plotted individually. Dashed lines represent line segments between nodes.

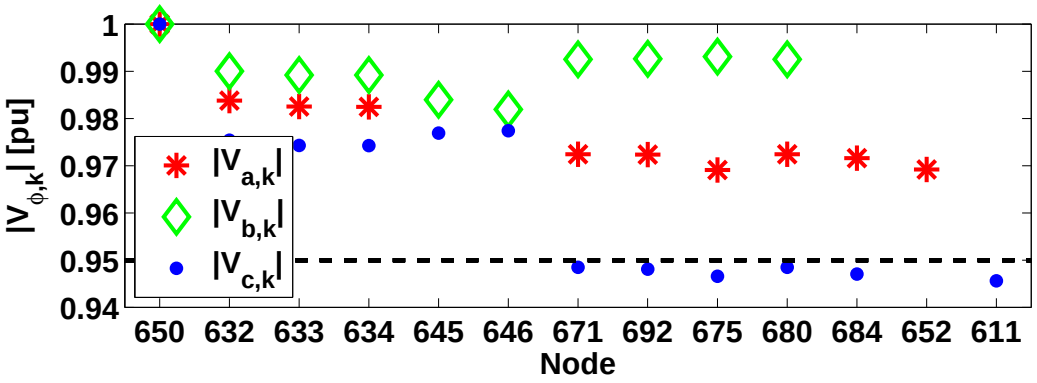



Figure 4.5: Phase $a$, $b$, and $c$ voltages magnitudes without control.

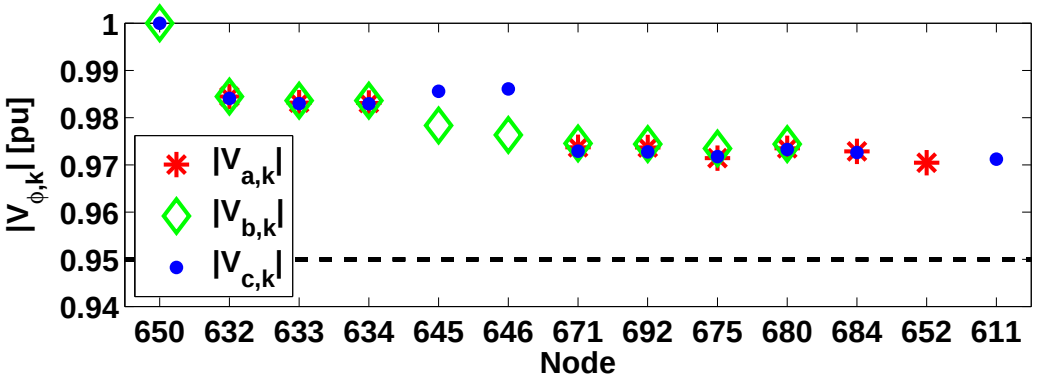



Figure 4.6: Phase $a$, $b$, and $c$ voltages magnitudes with control.

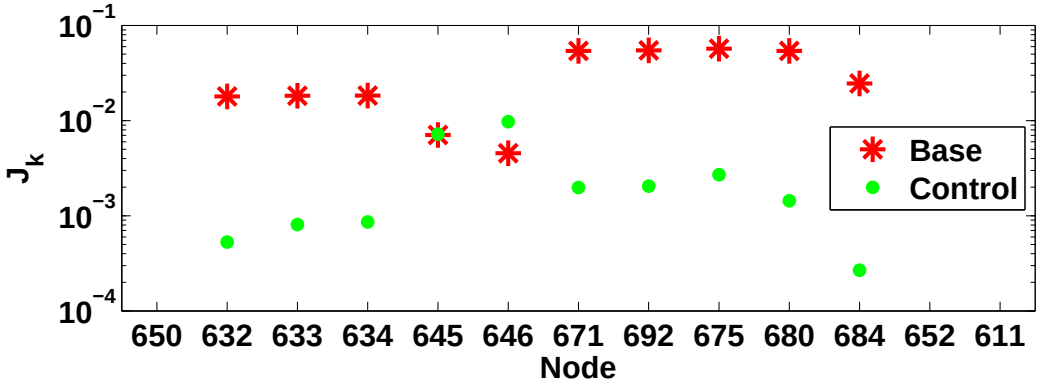



Figure 4.7: Phase voltage imbalance for all nodes, defined as the first term in the objective function of (4.23).

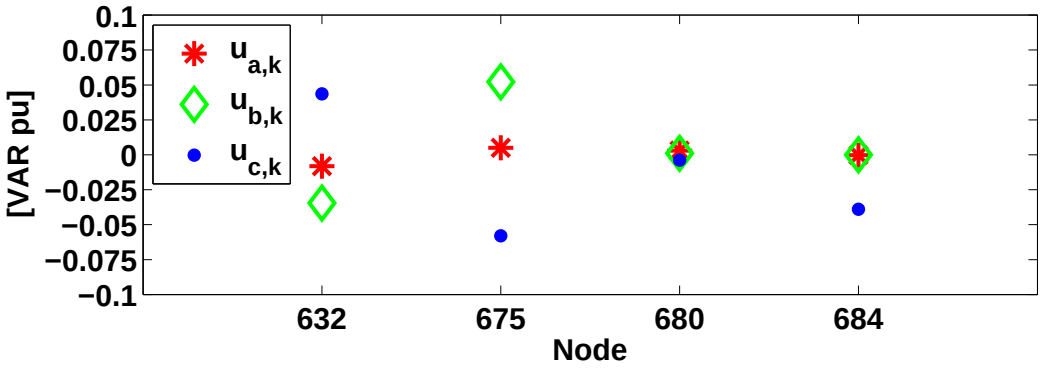



Figure 4.8: Optimal inverter VAR dispatch according to (4.23).

## 4.5 Concluding Remarks

This chapter considered optimization of three phase unbalanced distribution systems. In order to achieve this, I utilized a novel linearized model of distribution system power flow that maps real and reactive power injections into squared voltage magnitude differences. This approximate model can be viewed as an extension of the *LinDistFlow* [19] linear model to unbalanced distribution systems. The model was also used to give insight into an interesting phenomena regarding voltage rises on lightly loaded phases. As was discussed in Section 4.4, a rise in voltage magnitude in one phase can now be attributed to the fact that off diagonal components of (4.20)-(4.21) have *opposite* signs of the diagonal components, indicating that large voltage drops in some phases actually contribute to voltage *rises* in others.

Using the linear approximate power flow model, I also developed an Optimal Power Flow (OPF) program to control reactive power of DER to drive system voltages to within a $\pm 5\%$ threshold of 1 p.u., while simultaneously minimizing the squared Euclidean distance between squared voltage magnitudes at each node. This approach resulted in voltages that were much more balanced at each node, compared to the uncontrolled case. Although the objective considered in this work was to balance feeder voltages, the derived model is capable of optimizing over a variety of objectives as the equality constraints are now *linear*.

Having derived a suitable linearization for unbalanced power flow, I desire to extend the results of Chapters 2 and 3 to three phase systems. Apart from ES, I plan to conduct additional research aimed at exploring other useful applications of three phase unbalanced OPF driven by the new approximate model such as: voltage reference tracking, battery and electric vehicle charging, load forecasting, and state estimation.

# Chapter 5

# Conclusions

This work focused on the development of an approach to conduct model-free optimization of Distributed Energy Resources in electric power distribution systems. Initially, for radial and balanced distribution systems, an *Extremum Seeking* approach was utilized to enable distributed optimization of reactive power assets, followed by optimization of both real and reactive power assets. Finally, as a necessary step to lay the groundwork to extend the ES approach to unbalanced systems, a novel linearization of 3 phase power flow was derived and tested in an OPF formulation.

Chapter 2, which explored distributed model-free optimization of distribution systems using reactive power assets, presented two contributions. First, for balanced radial distribution systems, I derived conditions that guarantee feeder real and reactive power flows are convex and *squared* voltage magnitudes are concave with respect to injected reactive powers anywhere on a feeder. These conditions require that *reverse* real and reactive power flows and apparent power magnitudes remain below values that are extremely unlikely to occur on appropriately sized infrastructure. These results are based on the exact balanced distribution power flow equations (i.e. no approximations are required). The second major result was to demonstrate that ES control can manage distributed reactive power resources to perform optimal voltage-constrained real power minimization. This optimization is capable of operating in real time, without knowledge of any system models and with purely local decision-making. This work constitutes an important step towards practical implementation of distribution optimal power flow. While several existing studies already consider distributed and model-free voltage regulation, this contribution allows for a variety of objectives to be optimized, while ensuring voltages remain acceptable.

Chapter 3 considered distributed model-free optimization of distribution systems using four-quadrant-capable DER. A 2 dimensional *Extremum Seeking* control algorithm was employed to manage both the real power and reactive power output of controllable resources. While previous efforts utilized a sinusoidal probe to control only reactive power. In this work, I utilized the orthogonal sinusoid of the same frequency to allow for *simultaneous* control of inverter real and reactive power. In simulations I demonstrated distribution feeder substation real power and voltage reference tracking using PV systems managed by 2-D ES controllers,

which essentially allows the distribution feeder to emulate a (P,V) bus when viewed from the perspective of the transmission system operator. With this work, I have shown that model-free and distributed control algorithms can optimally provide regulation services to the bulk grid while maintaining internal voltage stability in the distribution system.

In this manuscript, I focused on applications with independent controllers that require relatively little communication. However, centralized multivariable ES may have better performance [14]. The convergence results still hold for this application, and in situations where high amounts of communication and a centralized architecture are acceptable, a multivariable approach may be preferable.

Although the specifics of the hardware providing optimal real and reactive power support were not considered in the analysis and simulation sections, the ES control approach could be utilized by advanced power inverters associated with PV, electric vehicle, and battery storage systems. Such DER have the potential to modulate their power outputs on timescales suitable for ES control and can either provide their own independent probes and/or share probing responsibilities with neighbors. However, it is also possible to extend the approach to support equipment incapable of actuating on timescales required for ES probing, such as demand response assets. To do so, it would be necessary to utilize the probing signal from another piece of hardware such as nearby DER capable of probing, or a dedicated probing resource. Additionally, the resolution of real-time feedback measurements also presents important design considerations. In my research, I ran simulations with small probing amplitudes to allow, potentially, small rooftop inverters to participate in the control effort. However, if the resolutions of substation real power and feeder voltage measurements are poor, than it may not be possible to have these units probe independently, as their small dither signals might be imperceptible in feedback measurements. As a work-around to this issue, one could coordinate smaller DER resources to probe as a collective unit, or "piggyback" on probes already in the system. These probes could originate from dedicated probing resources, which would need to be installed at several locations in a distribution system, or could come from larger resources that are attempting to optimize their own contributions to the grid. I intend to explore these ideas during my postdoctoral fellowship.

Chapter 4 constitutes the first effort to extend the ES control approach to optimize three phase unbalanced distribution systems. In order to achieve this, I derived a novel linearized model of distribution system power flow that maps real and reactive power injections into squared voltage magnitude differences. This approximate model can be viewed as an extension of the *LinDistFlow* [19] linear model to unbalanced distribution systems. The model was also used to give insight into an interesting phenomena regarding voltage rises on lightly loaded phases. As was discussed in Section 4.4, a rise in voltage magnitude in one phase can now be attributed to the fact that off diagonal components of (4.20)-(4.21) have *opposite* signs of the diagonal components, indicating that large voltage drops in some phases actually contribute to voltage *rises* in others. Using the linear approximate power flow model, I also developed an Optimal Power Flow (OPF) program to control reactive power of DER to drive system voltages to within a $\pm 5\%$ threshold of 1 p.u., while simultaneously minimizing the squared Euclidean distance between squared voltage magnitudes at each node.

This approach resulted in voltages that were much more balanced at each node, compared to the uncontrolled case. Although the objective considered in this work was to balance feeder voltages, the derived model is capable of optimizing over a variety of objectives as the equality constraints are now *linear*. Although the intent of this piece of research was to extend the ES control approach to unbalanced systems, I believe the 3-phase OPF driven by this unbalanced power flow approximation also warrants further study. I plan to conduct additional research aimed at exploring other useful applications including: voltage reference tracking, battery and electric vehicle charging, load forecasting, and state estimation.

Although we have derived a linear approximation that performs well when incorporated into a classical OPF, much work remains to transition ES control from balanced to unbalanced formulations. From an analytical standpoint, one still has to argue that the linear behavior of the model dominates other nonlinearities during normal operations of distribution systems. Such an argument will be necessary to claim that ES will work when managing DER in a simulation that uses un-approximated power flow equations (and, by extension, when ES is deployed to manage physical DER). I believe that there is also an oppurtunity to improve the ES algorithm itself. Using ES to control both real and reactive power contributions from up to 3 phases yields 6 possible control channels *per controllable device*. Although it would be possible to use 3 unique probes per node to accomplish full real and reactive power control across all phases, I believe, using intuition drawn from the spherical coordinate system, that it may be possible to reduce this number to 2 probes and smartly design their frequencies so that the product of sinusoidal terms (e.g. $\cos\phi\cos\psi$) results in a unique probe. This tradeoff would increase the complexity in designing the probing frequencies for a distribution system, but would reduce the number of probes within the system.

# References


[1] E M Stewart et al. *Analysis of High-Penetration Levels of Photovoltaics into the Distribution Grid on Oahu, Hawaii, Detailed Analysis of HECO Feeder WF1*. Tech. rep. NREL subcontract report NREL/SR-5500-54494, 2013.

[2] Zhan Shen and Mesut E Baran. "Gradient based centralized optimal Volt/Var control strategy for smart distribution system". In: *Innovative Smart Grid Technologies (ISGT), 2013 IEEE PES*. IEEE. 2013, pp. 1–6.

[3] Masoud Farivar et al. "Inverter VAR control for distribution systems with renewables". In: *IEEE International Conference on Smart Grid Communications (SmartGridComm)*. IEEE. 2011, pp. 457–462.

[4] Albert Lam et al. "Optimal distributed voltage regulation in power distribution networks". In: *arXiv preprint arXiv:1204.5226* (2012).

[5] Emiliano Dall'Anese, Georgios B Giannakis, and Bruce F Wollenberg. "Optimization of unbalanced power distribution networks via semidefinite relaxation". In: *North American Power Symposium (NAPS), 2012*. IEEE. 2012, pp. 1–6.

[6] Konstantin Turitsyn et al. "Options for control of reactive power by distributed photovoltaic generators". In: *Proceedings of the IEEE* 99.6 (2011), pp. 1063–1073.

[7] Na Li, Guannan Qu, and Munther Dahleh. "Real-time decentralized voltage control in distribution networks". In: *Communication, Control, and Computing (Allerton), 2014 52nd Annual Allerton Conference on*. IEEE. 2014, pp. 582–588.

[8] Brett Robbins, Christoforos N Hadjicostis, Alejandro D Domínguez-García, et al. "A two-stage distributed architecture for voltage control in power distribution systems". In: *Power Systems, IEEE Transactions on* 28.2 (2013), pp. 1470–1482.

[9] Baosen Zhang, Alejandro D Dominguez-Garcia, and David Tse. "A local control approach to voltage regulation in distribution networks". In: *North American Power Symposium (NAPS), 2013*. IEEE. 2013, pp. 1–6.

[10] JW Smith et al. "Smart inverter volt/var control functions for high penetration of PV on distribution systems". In: *IEEE Power Systems Conference and Exposition (PSCE)*. IEEE. 2011, pp. 1–6.

[11] Kartik B Ariyur and Miroslav Krstic. *Real-time optimization by extremum-seeking control*. John Wiley & Sons, 2003.

[12] Chunlei Zhang et al. "Source seeking with non-holonomic unicycle without position measurement and with tuning of forward velocity". In: *Systems & Control Letters* 56.3 (2007), pp. 245–252.

[13] Daniel Brian Arnold. "Control of a non-holonomic unicycle via extremum seeking". MA thesis. University of California, San Diego, 2006.

[14] Azad Ghaffari, Sridhar Seshagiri, and Miroslav Krstić. "Multivariable maximum power point tracking for photovoltaic micro-converters using extremum seeking". In: *Control Engineering Practice* 35 (2015), pp. 83–91.

[15] Aboozar Ghaffari, Miroslav Krstic, and Saradhi Seshagiri. "Power optimization and control in wind energy conversion systems using extremum seeking". In: *Control Systems Technology, IEEE Transactions on* 22.5 (2014), pp. 1684–1695.

[16] Azao Ghaffari, Miroslav Krstic, and Sridhar Seshagiri. "Extremum seeking for wind and solar energy applications". In: *Mechanical Engineering* 136.3 (2014), S13.

[17] Nick J Killingsworth et al. "HCCI engine combustion-timing control: Optimizing gains and fuel consumption via extremum seeking". In: *IEEE Transactions on Control Systems Technology* 17.6 (2009), pp. 1350–1361.

[18] *Rule 21 Smart Inverter Working Group Technical Reference Materials*. `http://www.energy.ca.gov/electricity_analysis/rule21/`. [Online; accessed Sept. 28-2015].

[19] Mesut E Baran and Felix F Wu. "Optimal sizing of capacitors placed on a radial distribution system". In: *IEEE Transactions on Power Delivery* 4.1 (1989), pp. 735–743.

[20] Musse Mohamud Ahmed and WL Soo. "Power line carrier (PLC) based communication system for distribution automation system". In: *Power and Energy Conference, 2008. PECon 2008. IEEE 2nd International*. IEEE. 2008, pp. 1638–1643.

[21] Donald J Hammerstrom et al. *Detection of Periodic Beacon Loads in Electrical Distribution Substation Data*. Tech. rep. PNNL-15854, 2006.

[22] Hassan K Khalil and JW Grizzle. *Nonlinear systems*. 3rd. Prentice hall Upper Saddle River, 2002, pp. 402–411.

[23] William H Kersting. *Distribution system modeling and analysis*. 2nd. CRC press, 2012, pp. 328–330.

[24] *PG&E Direct Access Customer Class Load Profile*. `http://www.pge.com/nots/rates/006f1c4_class_load_prof.shtml`. [Online; accessed July-2014].

[25] *The Pecan Street Project*. `http://www.pecanstreet.org/`. [Online; accessed May-2015].

[26] *IEEE Distribution Test Feeders*. `http://ewh.ieee.org/soc/pes/dsacom/testfeeders/index.html`. [Online; accessed May-2015].

[27] *PJM Ancillary Sevices*. `http://www.pjm.com/markets-and-operations/ancillary-services.aspx`. [Online; accessed Oct. 1-2015].

[28] Raphael Louca, Peter Seiler, and Eilyan Bitar. "Nondegeneracy and Inexactness of Semidefinite Relaxations of Optimal Power Flow". In: *arXiv* 1441.4663v1 (2014).

# Bibliography

[11] Kartik B Ariyur and Miroslav Krstic. *Real-time optimization by extremum-seeking control*. John Wiley & Sons, 2003.

[22] Hassan K Khalil and JW Grizzle. *Nonlinear systems*. 3rd. Prentice hall Upper Saddle River, 2002, pp. 402–411.

[23] William H Kersting. *Distribution system modeling and analysis*. 2nd. CRC press, 2012, pp. 328–330.

[29] Leonard L Grigsby. *Electric power generation, transmission, and distribution*. CRC press, 2012.

[30] David G Luenberger and Yinyu Ye. *Linear and Nonlinear Programming*. 3rd ed. Springer, 2008.

# Appendix A

# Appendix

## A.1 Proof of Theorem 1

Consider a distribution feeder represented by $T$. Let $m$ represent the order (i.e. number of nodes) of $T$ and let $u$ be the vector of all controllers ($u_i$) at nodes in $H$, where $u = [u_1, \ldots, u_m]^T \in \Re^{m\times 1}$. Without loss of generality, we assume a controller exists at every node in $H$. For a node $i \in H$, denote the Hessians of $P_i$ and $Q_i$ with respect to $u$ as $\nabla_u^2 P_i \in \Re^{m\times m}$, $\nabla_u^2 Q_i \in \Re^{m\times m}$ respectively. In addition, denote the Hessian of $y_i$ with respect to $u$ as $\nabla_u^2 y_i \in \Re^{m\times m}$. Finally, denote the gradients of $P_i, Q_i$, and $y_i$ with respect to $u$ as $\nabla_u P_i \in \Re^{1\times m}$, $\nabla_u Q_i \in \Re^{1\times m}$, and $\nabla_u y_i \in \Re^{1\times m}$ respectively. The following theorem outlines the regions under which the Hessians $\nabla_u^2 P_i$ and $\nabla_u^2 Q_i$ are positive semidefinite and $\nabla_u^2 y_i$ are negative semidefinite.

*Proof.* Proceeds by induction beginning from the ends of the feeder, and infinite node assumption ($y_0$ evolves independently and on a timescale slower than our control actions). To prove the induction step, consider the nodes that makeup the $k^{th}$ level of the graph $T$ (i.e. the set of nodes which are $k$ line segments away from the root of $T$). In a radial feeder, these nodes are all children of nodes at level $k-1$, which are one segment close to the substation than nodes at level $k$. Considering just the nodes and line segments that link level $k-1$ to level $k$, these nodes and line segments define a forest of rooted tree graphs of maximum height 1. Define this rooted forest as $T_k = (H_k, E_k)$ where the root nodes (all nodes at level $k-1$ of $T$) are indexed by $i$. The induction hypothesis assumes the following are true for all nodes at level $k$ (or all nodes $j \in H_k, j \neq i$):

$$v^T \nabla_u^2 P_j v \geq 0 \tag{A.1}$$

$$v^T \nabla_u^2 Q_j v \geq 0 \tag{A.2}$$

$$\alpha_j v^T \nabla_u^2 P_j v \geq v^T \nabla_u^2 Q_j v \tag{A.3}$$

$$\beta_j v^T \nabla_u^2 Q_j v \geq v^T \nabla_u^2 P_j v. \tag{A.4}$$

For the purposes of the proof, it is also necessary to satisfy the following condition $\forall(i,j) \in E_k$:

$$-\frac{P_j^2 + Q_j^2}{y_j^2 - \left(r_{ij}^2 + x_{ij}^2\right)\left(P_j^2 + Q_j^2\right)} v^T \nabla_u^2 y_i v \geq 0 \tag{A.5}$$

Condition (A.5) implies two allowable regions of $P_j$ and $Q_j$ depending on the sign of $v^T \nabla_u^2 y_j v$. If the Hessian of $y_i$ is positive semidefinite, then $P_j = Q_j = 0$. On the other hand, if the Hessian term is negative semidefinite, then (A.5) is satisfied for any $P_j$ and $Q_j$ that also satisfies condition **C3**.

We begin the proof of the induction step with writing the Hessians of $P_i$, $Q_i$, and $y_i$ with respect to all controllers in $H$ (i.e. all controllers associated with nodes in the *entire* feeder, or $T$). As node $i$ is the root of $T_k$ and $T_k$ has a height of 1, the Hessians $\nabla_u^2 P_i$, $\nabla_u^2 Q_i$, and $\nabla_u^2 y_i$ can be expressed in terms of $\nabla_u^2 P_j$, $\nabla_u^2 Q_j$, and $\nabla_u^2 y_j$ for all $j \in H_k, j \neq i$.

$$\nabla_u^2 P_i = \sum_{j:(i,j)\in E_k} \nabla_u^2 P_j + \frac{2r_{ij}}{y_j}\Lambda_j + \frac{2r_{ij}}{y_j}\left(P_j \nabla_u^2 P_j + Q_j \nabla_u^2 Q_j\right) - \frac{r_{ij}}{y_j^2}(P_j^2 + Q_j^2)\nabla_u^2 y_j \tag{A.6}$$

$$\nabla_u^2 Q_i = \sum_{j:(i,j)\in E_k} \nabla_u^2 Q_j + \frac{2x_{ij}}{y_j}\Lambda_j + \frac{2x_{ij}}{y_j}\left(P_j \nabla_u^2 P_j + Q_j \nabla_u^2 Q_j\right) - \frac{x_{ij}}{y_j^2}(P_j^2 + Q_j^2)\nabla_u^2 y_j \tag{A.7}$$

$$\begin{aligned}\nabla_u^2 y_i = &\left(1 - \frac{r_{ij}^2 + x_{ij}^2}{y_j^2}(P_j^2 + Q_j^2)\right)\nabla_u^2 y_j + \frac{2(r_{ij}^2 + x_{ij}^2)}{y_j}\Lambda_j + \left(2r_{ij} + 2\frac{r_{ij}^2 + x_{ij}^2}{y_j}P_j\right)\nabla_u^2 P_j \\ &+ \left(2x_{ij} + 2\frac{r_{ij}^2 + x_{ij}^2}{y_j}Q_j\right)\nabla_u^2 Q_j \quad \forall(i,j) \in E_k,\end{aligned} \tag{A.8}$$

where

$$\begin{aligned}\Lambda_j = &\left[\left(\nabla_u P_j - \frac{P_j}{y_j}\nabla_u y_j\right)^T \left(\nabla_u P_j - \frac{P_j}{y_j}\nabla_u y_j\right)\right. \\ &\left. + \left(\nabla_u Q_j - \frac{Q_j}{y_j}\nabla_u y_j\right)^T \left(\nabla_u Q_j - \frac{Q_j}{y_j}\nabla_u y_j\right)\right].\end{aligned} \tag{A.9}$$

Using a bit of tedious algebra, it can be shown that application of the induction hypothesis (**C1** - **C3**) and conditions (A.1) - (A.4) to the system (A.6) - (A.8) yields the following results:

$$v^T \nabla_u^2 P_i v \geq \sum_{j:(i,j)\in E_k} -r_{ij}\left(\frac{P_j^2 + Q_j^2}{y_j^2 - (P_j^2 + Q_j^2)(r_{ij}^2 + x_{ij}^2)}\right) v^T \nabla_u^2 y_i v \tag{A.10}$$

$$v^T \nabla_u^2 Q_i v \geq \sum_{j:(i,j)\in E_k} -x_{ij} \left( \frac{P_j^2 + Q_j^2}{y_j^2 - (P_j^2 + Q_j^2)(r_{ij}^2 + x_{ij}^2)} \right) v^T \nabla_u^2 y_i v \tag{A.11}$$

$$v^T \nabla_u^2 y_i v \geq \left( 1 - \frac{P_j^2 + Q_j^2}{y_j^2} \left( r_{ij}^2 + x_{ij}^2 \right) \right) v^T \nabla_u^2 y_j v$$
$$\forall (i,j) \in E_k, j \in H_k, j \neq i. \tag{A.12}$$

Application of (A.5) to the system (A.10) - (A.11) satisfies the first two components of the induction hypothesis ((A.1) - (A.2)). Eq. (A.12) is proven as a consequence of the induction hypothesis and will be useful later in the proof. Conditions (A.3) - (A.4) can be proven by showing $\alpha_i v^T \nabla_u^2 P_i v - v^T \nabla_u^2 Q_i v \geq 0$ and $\beta_i v^T \nabla_u^2 Q_i v - v^T \nabla_u^2 P_i v \geq 0$:

$$\alpha_i v^T \nabla_u^2 P_i v - v^T \nabla_u^2 Q_i v = \sum_{j:(i,j)\in E_k} \left( \alpha_i + 2\frac{P_j}{y_j} \left( \alpha_i r_{ij} - x_{ij} \right) \right) v^T \nabla_u^2 P_j v$$
$$+ \left( 2\alpha_i r_{ij} \frac{Q_j}{y_j} - \left( 1 + 2x_{ij} \frac{Q_j}{y_j} \right) \right) v^T \nabla_u^2 Q_j v + \left( \alpha_i r_{ij} - x_{ij} \right) \left( -\frac{P_j^2 + Q_j^2}{y_j^2} v^T \nabla_u^2 y_j v + \frac{2}{y_j} \Lambda_j \right) \tag{A.13}$$

$$\beta_i v^T \nabla_u^2 Q_i v - v^T \nabla_u^2 P_i v = \sum_{j:(i,j)\in E_k} \left( \beta_i + 2\frac{Q_j}{y_j} \left( \beta_i x_{ij} - r_{ij} \right) \right) v^T \nabla_u^2 Q_j v$$
$$+ \left( 2\beta_i x_{ij} \frac{P_j}{y_j} - \left( 1 + 2r_{ij} \frac{P_j}{y_j} \right) \right) v^T \nabla_u^2 P_j v + \left( \beta_i x_{ij} - r_{ij} \right) \left( -\frac{P_j^2 + Q_j^2}{y_j^2} v^T \nabla_u^2 y_j v + \frac{2}{y_j} \Lambda_j \right). \tag{A.14}$$

Again, using the induction hypothesis and the conditions of the theorem on (A.13) - (A.14), the following can be shown:

$$\alpha_i v^T \nabla_u^2 P_i v - v^T \nabla_u^2 Q_i v \geq - \sum_{j:(i,j)\in E_k} \left( \alpha_i r_{ij} - x_{ij} \right) \frac{P_j^2 + Q_j^2}{y_j^2 - (r_{ij}^2 + x_{ij}^2)(P_j^2 + Q_j^2)} v^T \nabla_u^2 y_i v \tag{A.15}$$

$$\beta_i v^T \nabla_u^2 Q_i v - v^T \nabla_u^2 P_i v \geq - \sum_{j:(i,j)\in E_k} \left( \beta_i x_{ij} - r_{ij} \right) \frac{P_j^2 + Q_j^2}{y_j^2 - (r_{ij}^2 + x_{ij}^2)(P_j^2 + Q_j^2)} v^T \nabla_u^2 y_i v. \tag{A.16}$$

Since $(\alpha_i x_{ij} - r_{ij}) \geq 0$ and $(\beta_i r_{ij} - x_{ij}) \geq 0$, condition (A.5) shows that (A.15) - (A.16) are positive semidefinite which validates (A.3) - (A.4) and completes the induction step.

To satisfy the basis step of the induction, consider the maximum height of the tree $T$, denoted by $h$. All nodes at level $h$ are leaves of $T$. For these nodes (2.1) - (2.2) become:

$$P_j = p_j, \quad Q_j = q_j + u_j, \quad j \in L \tag{A.17}$$

Where $L$ is the set of all nodes at level $h$. Inspection of (A.17) shows that $\nabla_u^2 P_j$ and $\nabla_u^2 Q_j$ are matrices with 0 entries, which satisfy the conditions of the induction with $\alpha_j = \beta_j = 0$.

It is quite possible that nodes at levels less than $h$ will also be leaves of $T$. However, as (A.17) shows, these nodes do not contribute any terms of the form: $v^T \nabla_u^2 P_j v, v^T \nabla_u^2 Q_j v$ (as these are equal to 0) to the Hessians of their parent nodes and can directly be incorporated into the induction step.

It remains to be shown that the result **R3** is satisfied. For any node $i$ in $T$ which is the parent of another node $j$, we have already proven (A.12) is globally satisfied. Consider the voltage Hessian at node 0. Our initial assumption that $y_0$ is unchanging with respect to control decisions implies that $v^T \nabla_u^2 y_0 v = 0$. As the quantity: $1 - \frac{(r_{ij}^2 + x_{ij}^2)(P_j^2 + Q_j^2)}{y_j^2} \geq 0$ for all $(i, j) \in E$, condition (A.12) implies the Hessians of all nodal voltages with respect to $u$ are negative semidefinite. □

## A.2 Discussion of Objective Function for Eq. (3.43)

Here I discuss the choice of Eq. (3.43) as the objective function to enable feeder head real power and voltage target tracking, as opposed to a more conventional quadratic form. The difference in performance can be attributed to the presence of the loss terms of Eqs. (3.30)–(3.32) (and subsequently the constant terms of the approximate power flow model in Eqs. (3.35)–(3.37)). As was previously mentioned, simulation experiments of the quadratic objective consistently resulted in convergence to larger neighborhoods around $(u^*, v^*)$, leading to larger tracking errors. The following analysis on a simplified problem is intended to motivate the reasoning behind this observed phenomena.

Consider a simplified ES scheme outlined in Fig. A.1. This block diagram features a single ES loop without high and low pass filters. Let us consider an objective of the form: $J(u) = (P_0 - P_t)^2$, where $P_0 = u + g$. This model for $P_0$ represents a 2 node feeder, where $g$ accounts for the real power losses. Defining the error system: $\tilde{u} = \hat{u} - P_t$, we can expand the objective function:

$$J(u) = (\tilde{u} + g)^2 + a^2 \cos^2(\omega t) + 2a \cos(\omega t)\,(\tilde{u} + g)\,. \tag{A.18}$$

Demodulating $J(u)$ and passing the resulting signal through the integrator block of Fig. A.1 results in the following equation governing the error dynamics of the ES controller:

$$\dot{\tilde{u}} = -k \cos(\omega t)\left[(\tilde{u} + g)^2 + a^2 \cos^2(\omega t)\right] - k \cos(\omega t)\left[2a \cos(\omega t)\,(\tilde{u} + g)\right]. \tag{A.19}$$

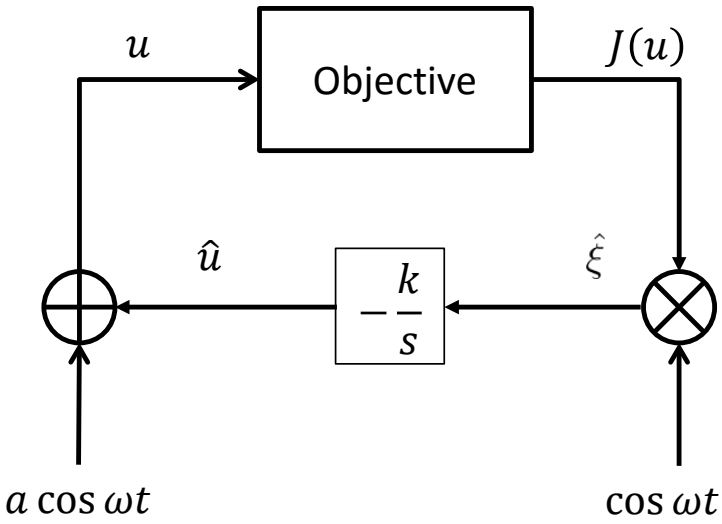



Figure A.1: Simplified ES block diagram. High pass filter before demodulation and low pass filter after demodulation are neglected.

We now define the time constant $\tau = \omega t$ and integrate Eq. (A.19) over the time period 0 to $\frac{\omega}{2\pi}$, which results in the averaged error dynamics of $\tilde{u}$:

$$\dot{\tilde{u}}_{av} = -\frac{ka}{2\pi}\left(\tilde{u}_{av} + g\right), \tag{A.20}$$

where $k$ and $a$ are positive constants. Let us assume for the moment that $g$ is constant. This means that $\tilde{u}_{av}$ will not converge to the origin. Rather, when $\tilde{u}_{av}$ dominates $g$ then $\tilde{u}_{av}$ will decrease, but will subsequently stop decreasing as $g$ becomes greater than $\tilde{u}_{av}$. This implies convergence of $\tilde{u}_{av}$ to a ball around the origin, the size of which is determined by $g$. Such an explanation is consistent with observed simulation results when using a quadratic objective function, where controllers would converge to a larger neighborhood around the tracking signals compared to results obtained using the objective function of Eq. (3.43).